General Disclaimer

One or more of the Following Statements may affect this Document

- This document has been reproduced from the best copy furnished by the organizational source. It is being released in the interest of making available as much information as possible.

- This document may contain data, which exceeds the sheet parameters. It was furnished in this condition by the organizational source and is the best copy available.

- This document may contain tone-on-tone or color graphs, charts and/or pictures, which have been reproduced in black and white.

- This document is paginated as submitted by the original source.

- Portions of this document are not fully legible due to the historical nature of some of the material. However, it is the best reproduction available from the original submission.

Produced by the NASA Center for Aerospace Information (CASI)

EXPERIMENTS ON THE INJECTION AND CONTAINMENT OF ELECTRON CLOUDS IN A TOROIDAL APPARATUS

J.D. Daugherty, J.E. Eninger and G.S. Janes

RESEARCH REPORT 284
July 1968

supported by

UNITED STATES
ATOMIC ENERGY COMMISSION
NEW YORK OPERATIONS OFFICE
New York, New York 10014
NYO-3863-7

under Contract No. AT(30-1)-3863

NATIONAL AERONAUTICS AND SPACE ADMINISTRATION
GEORGE C. MARSHALL SPACE FLIGHT CENTER
Huntsville, Alabama

under Contract No. NAS 8-21392

AIR FORCE OFFICE OF SCIENTIFIC RESEARCH
OFFICE OF AEROSPACE RESEARCH
UNITED STATES AIR FORCE
Washington 25, D.C.

under Contract No. AF 49(638)-1553
Project Task: 9752-01

N69-13212
(ACCESSION NUMBER) (THRU) 1
(PAGES) (CODE) 25
NASA-CR-98158 (NASA CR OR TMX OR AD NUMBER) (CATEGORY)
FACILITY FORM 602

SEP 1968
RECEIVED
NASA STI FACILITY
INPUT BRANCH

AVCO EVERETT RESEARCH LABORATORY
A DIVISION OF AVCO CORPORATION

RESEARCH REPORT 284

EXPERIMENTS ON THE INJECTION AND CONTAINMENT OF ELECTRON CLOUDS IN A TOROIDAL APPARATUS

by

J. D. Daugherty, J. E. Eninger and G. S. Janes

AVCO EVERETT RESEARCH LABORATORY
a division of
AVCO CORPORATION
Everett, Massachusetts

July 1968

supported by

UNITED STATES
ATOMIC ENERGY COMMISSION
NEW YORK OPERATIONS OFFICE
New York, New York 10014
NYO-3863-7

under Contract No. AT(30-1)-3863

NATIONAL AERONAUTICS AND SPACE ADMINISTRATION
GEORGE C. MARSHALL SPACE FLIGHT CENTER
Huntsville, Alabama

under Contract No. NAS 8-21392

AIR FORCE OFFICE OF SCIENTIFIC RESEARCH
OFFICE OF AEROSPACE RESEARCH
UNITED STATES AIR FORCE
Washington 25, D. C.

under Contract No. AF 49(638)-1553
Project Task: 9752-01

PRECEDING PAGE BLANK NOT FILMED

ABSTRACT

Injection and containment of un-neutralized clouds of electrons has been accomplished with an azimuthally symmetric, toroidal, magnetic field. The confining magnetic field is produced within a conducting toroidal chamber. The induction of this magnetic field has been used to inject the electron cloud (inductive charging). Average electron densities of 4×10^9 cm^{-3} and peak electrostatic well depths of ≈ 400 kv have been achieved. Semi-empirical correlations are given which show the inductive charging scheme to be governed by an electron energy restriction and finally limited by the occurrence of anamolous crossed field beam noise. Stable equilibria, without the necessity of a rotational transform have been observed for times in excess of 60μ sec. Correlation of the containment time observations with the predictions of a theoretical model for an ion-diocotron wave instability shows that the containment time is governed by the rate of ionization of the residual neutral gas ($p > 10^{-7}$ torr) in the apparatus. The correlation of theory and experiment appear to confirm the theoretical prediction that significant fractional charge neutralization (in the range of 10% to 20%) can be stably contained. Interpretation of these results suggests that significant improvement in both electron cloud density and containment time should be possible.

PRECEDING PAGE BLANK NOT FILMED.

TABLE OF CONTENTS

1. INTRODUCTION

Experimental [1, 2] and theoretical [3, 4, 5] evidence suggests that unneutralized clouds of electrons can be confined by a toroidal magnetic field. Both the development of a means for generation and the demonstration of long term containment of stable electron clouds in toroidal configurations are necessary for demonstrating the feasibility of at least three new crossed-field electron devices having widely differing applications. These applications are a heavy ion accelerator, [2] a source of highly stripped heavy ions [6] and a solar flare proton radiation shield. [7]

The two main experimental research goals which must be achieved to make these crossed-field electron devices feasible are:

(1) development of a means to generate (inject) electron densities of between 10^{10} cm^{-3} and 10^{11} cm^{-3} and

(2) achievement of electron containment times of the order of 1 to 10 sec for the ion accelerator and ion source applications and of the order of 10^5 sec for the space radiation shield application.

In this paper, we present the results of our initial experiments on the injection and containment of electrons clouds in an azimuthally symmetric, toroidal apparatus. The device used for these experiments is the toroidal vacuum chamber shown on Fig. 1. We describe this apparatus in detail in Section 2.

The principle aim of the present experiments has been to study and develop the inductive charging method of electron injection. [1] The inductive

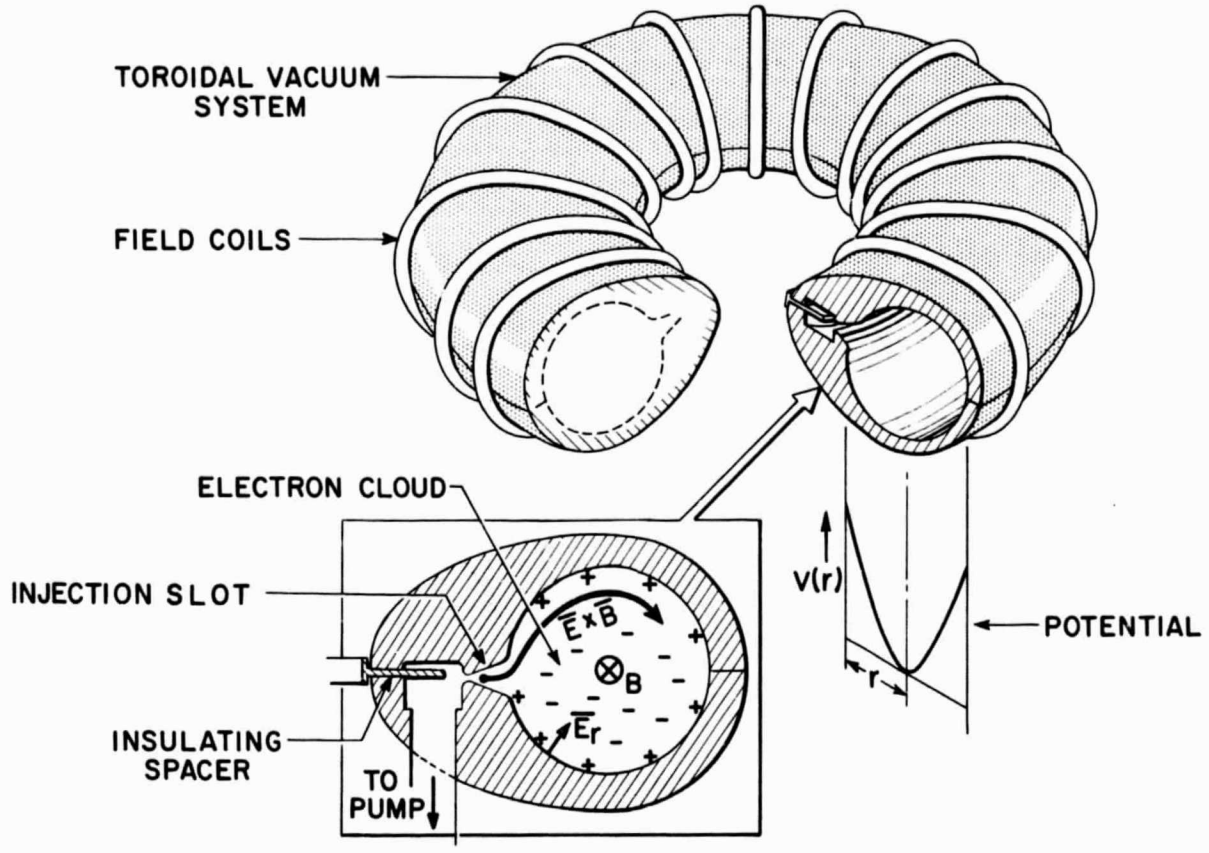

Fig. 1 Schematic diagram of the experimental torus. The torus is constructed of aluminum and can be evacuated to $\approx 10^{-7}$ torr. The magnetic field is induced by a capacitor bank discharge through the field coils shown. All magnetic flux enters the conducting torus through the insulated spacer shown.

charging method utilizes the energy flow occurring during the establishment of the containing magnetic field both to transport adiabatic[8] electrons into the device and to raise their potential energy. (i.e. create an electrostatic potential). This injection scheme is described in detail in Section 3.

In Section 3, we present the semi-empirical correlations found to govern our injection scheme. These limits are shown to arise from the occurrence of:

(1) a natural energy limitation for the injected electrons and,

(2) an anomalous noise or electron heating mechanism.

We believe the latter limitation to be the same anomalous electron heating phenomena that has been observed by previous researchers on crossed field switching[9] and microwave[10] devices. In Section 4 the two limits (1) and (2) are shown to combine to produce the result that the total injected charge (average electron density) is directly proportional to the injection cathode bias voltage. By means of our inductive charging scheme, we have achieved average electron densities of about 4×10^9 cm^{-3} at an average magnetic field of $B \approx 1.5$ kg. Means for achieving the goal of 10^{10} to 10^{11} cm^{-3} are discussed in Section 6.

The secondary objectives of our present experiments have been to demonstrate the existence of a toroidal equilibrium and to investigate the onset of an instability which is found to arise as the electron cloud progressively becomes neutralized via ionization of the residual background gas. Our experimental studies of electron cloud containment are discussed in Section 5. The experimental results confirm theoretical predictions[3] that despite gradient B and curvature drifts, electron cloud equilibria exist for

our toroidal apparatus without the necessity of a rotational transform.[11] We have found that our present containment times are in fact determined by the ionization of background neutral particles. With our present experimental pressure of $> 10^{-7}$ torr and our average electron densities of $\leq 4 \times 10^{9}$ cm^{-3} we have observed containment in excess of 60μ sec. The evidence shows that the injected electron cloud is stable until the degree of neutralization due to background gas ionization reaches some fraction ($\alpha = Z\,\bar{n}_i/\bar{n}_e$ = order of 10%) of the electron density. A theoretical model[12] is shown to correlate these experimental results. Implications of these results with respect to the proposed applications are discussed in Section 6.

2. EXPERIMENTAL APPARATUS AND DIAGNOSTICS

A. General Description

Figure 1 shows the apparatus with which we have been working. It consists of a toroidal, aluminum vacuum chamber which, at present, is capable of achieving a vacuum of the order of 10^{-7} torr. The major radius of this torus is 46 cm and the interior circular radius or minor radius is 10 cm. An azimuthally symmetric magnetic field is induced in the torus by means of a capacitor bank discharge through the field coils shown in Fig. 1. Typically the magnetic field rises to a maximum in less than 50 μ sec so that all of the magnetic field energy enters the interior of the conducting torus through a narrow circumferential gap filled with an insulating spacer (Fig. 1). Upon reaching the peak magnetic field, the field coils are "crowbarred" so that the magnetic field decays back to zero in about 0.7 ms. For such short time scales the skin depth in the aluminum is much less than the wall thickness. Thus the vacuum chamber acts as a "flux concentrator" and the magnetic field within the apparatus is aligned by the carefully machined, highly conducting, interior surfaces of the chamber. This familiar method of aligning pulsed magnetic fields assures that our experimental field lines are azimuthally symmetric independent of the exterior coil construction.

Figure 2 shows a schematic representation of the cross section of the apparatus. Two characteristic regions are evident. First, there is the compression chamber which has a circular cross section 10 cm in radius.

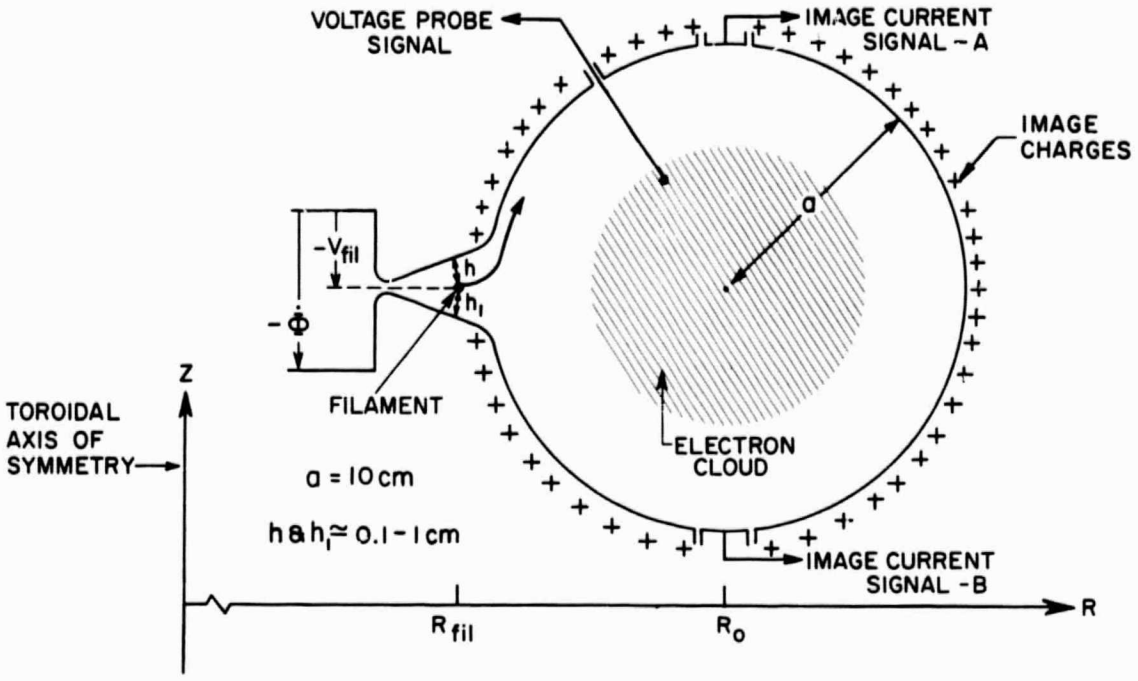

Fig. 2 Schematic representation of the cross section of the experimental apparatus. Electrons are emitted from the filament located in the electrostatically shielded tapered region on the left. Electrons are accumulated in the large circular compression chamber thereby forming a negative potential well. Characteristic dimensions, voltages, and diagnostics are shown schematically. The induction voltage $\dot{\Phi} \approx \dot{B}(R_o)\pi a^2$. The voltage probe which was connected to a high impedance measuring device and was only useful up to approximately 80 kv because of breakdown of its insulation. Above 80 kv, only the image current buttons could be used to measure the total charge in the system (see Fig. 3).

This is the region in which the injected electron charge is accumulated thereby forming a deep negative potential well. The second characteristic region is the tapered gap shown on the left in Fig. 2. In this gap, we have constructed an electron emitting cathode (filament) which encircles the major axis of the device. For the filament we have used a 0.5 mm diameter tungsten wire with an effective emitting length of about 170 cm.

B. An Electrostatic Design Consideration

The space charge electric field at the conducting wall of the compression chamber is approximately $E_o = Q/(2\pi\epsilon_o a)(2\pi R_o)$. Suppose that the filament were located in the compression chamber a distance h from the wall and biased negatively a voltage V_{fil}; then the biasing electric fields are of the order of V_{fil}/h. Therefore, if the induced space charge field E_o becomes comparable to the filament bias fields ($E_o \approx V_{fil}/h$) the filament can be cut off due to "back biasing". This electrostatic cutoff would limit the injected charge to roughly

$$Q \approx \left(\frac{a}{h}\right)\left((2\pi R_o)\ (2\pi\epsilon_o)\ V_{fil}\right) = \left(\frac{a}{h}\right) Q_o \qquad (1)$$

where R_o = major radius and a = minor radius. Q_o is a convenient abbreviation for the frequently appearing factor $(2\pi R_o)(2\pi\epsilon_o) V_{fil}$.

In the present configuration, the tapered gap was designed to decouple or shield the filament electric field from the more intense fields of the compression chamber and thus allow the injected charge to exceed the limit of Eq. (1). Tapering of the gap was used to effect a relatively smooth transition in these electric fields, and to thus minimize the electric field concentration occuring at the transition. We estimated the electrostatically limited charge that could be injected with this electrostatic shield by making

the simplest assumption--that of a uniform charge density in the compression chamber and in the gap. This limit is roughly

$$Q \approx \left(\frac{a}{h}\right)\left(\frac{a}{h_1}\right) Q_o \qquad (2)$$

where the characteristic dimension h_1 is as labeled on Fig. 2. Since a = 10 cm and we can make $h_1 < 1$ cm, Eq. (2) predicts that provision for electrostatic shielding could result in over a factor of 10 increase in total injected charge for a given filament voltage. However, the actual improvement attained was less than indicated by Eq. (2) because of the occurrence of a combination of other injection limitations to be described in Section 3.

C. Diagnostics

Figure 2 also shows schematically the two diagnostic tools that we have used to obtain measurements both during and after injection. The first of these tools is a movable voltage probe. This probe is simply a wire with a quartz insulating cover. The wire is exposed to the electron cloud at the end of the quartz insulation. Connection of the probe wire to an external, high impedance, measuring circuit reduced loading effects and permits a direct measurement of the cloud potential. This voltage probe has performed very well without breakdown at total well potentials up to 80 kv. From correlation of these voltage measurements with total charge measurements, we justify our inference of potentials above 80 kv (Section 4).

Our second diagnostic tool, the so called current button, has proved extremely useful in either of two modes of operation. As diagrammed in Fig. 2, the current button is a small (≈ 3 cm^2) isolated section of the compression chamber wall. Since the un-neutralized electrons induce a

positive surface (or image) charge in the walls, the image current which flows to this isolated section can be measured and interpreted. The two modes of operation for this diagnostic tool are as shown in Fig. 3. First, we can measure the current which flows to the device during injection as shown in Fig. 3a. This smooth trace was obtained with a simple two stage filter ($RC \approx .1$ to $.2\mu$ sec) which eliminated high frequency noise. In this figure we observe the image current rising, reaching a plateau, and subsequently falling or cutting off--these injection details are discussed in Section 3. Integration of this image current signal produces a signal proportional to the total charge injected into the device.

In order to measure the instantaneous injection current as shown in Fig. 3a, it was necessary to bias the current button with a relatively large negative voltage. If such a negative bias was not applied, electron losses from the injection beam (Section 3) produced a signal which swamped the true image charge signal. Figure 4 shows a typical curve of total measured charge versus current button bias. The plateau reached at high bias level yields the measurement of the actual injected charge. This plateau was reached only for bias voltages several times the filament bias voltage.

In Fig. 3a we observe waves occuring after injection cutoff. From measurements with current buttons located azimuthally about the major axis of the torus these waves have been observed to be azimuthally synchronous--i.e. there is no wave propagation parallel to the magnetic field. Thus the waves have been identified as diocotron[4] waves propagating perpendicular to the magnetic field.

At this very early time in the experimental cycle (5 to 10 μ sec after initiation of the experiment) the measured diocotron waves do not arise from

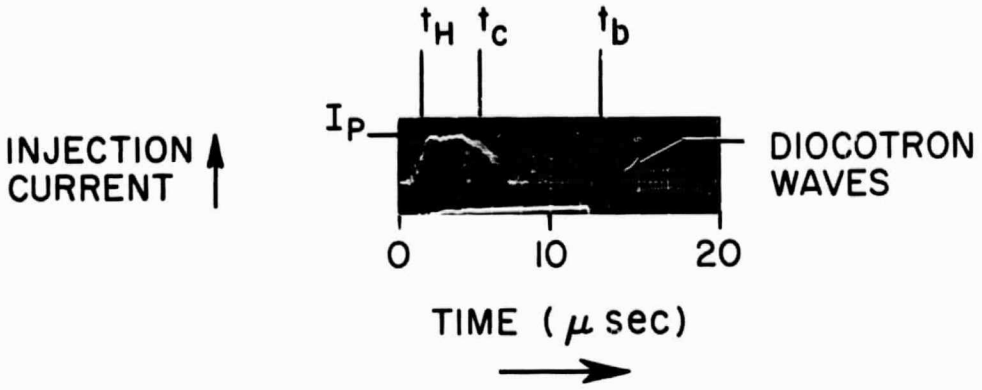

Fig. 3a

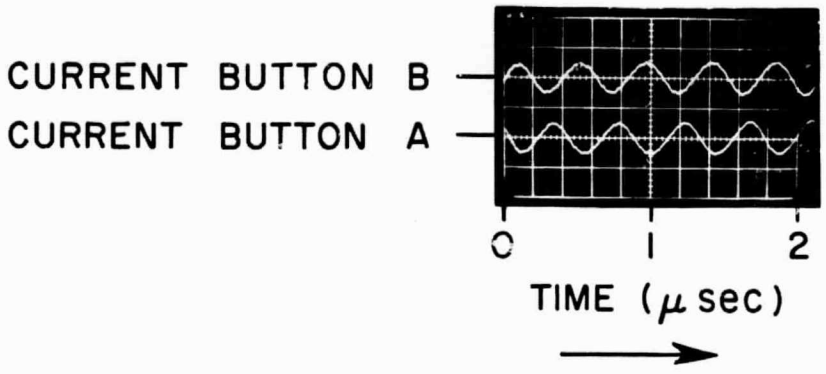

Fig. 3b

Fig. 3 Oscilloscope traces demonstrating image charge measurements obtained using the current buttons shown schematically in Fig. 2. Figure 3a shows the measured injection current which may be integrated to obtain a measure of the total injected charge. Figure 3b shows the diocotron waves which are also observed using current buttons. The frequency of these waves may be related to the total injected charge (Eq. (3)).

A8176
A8175

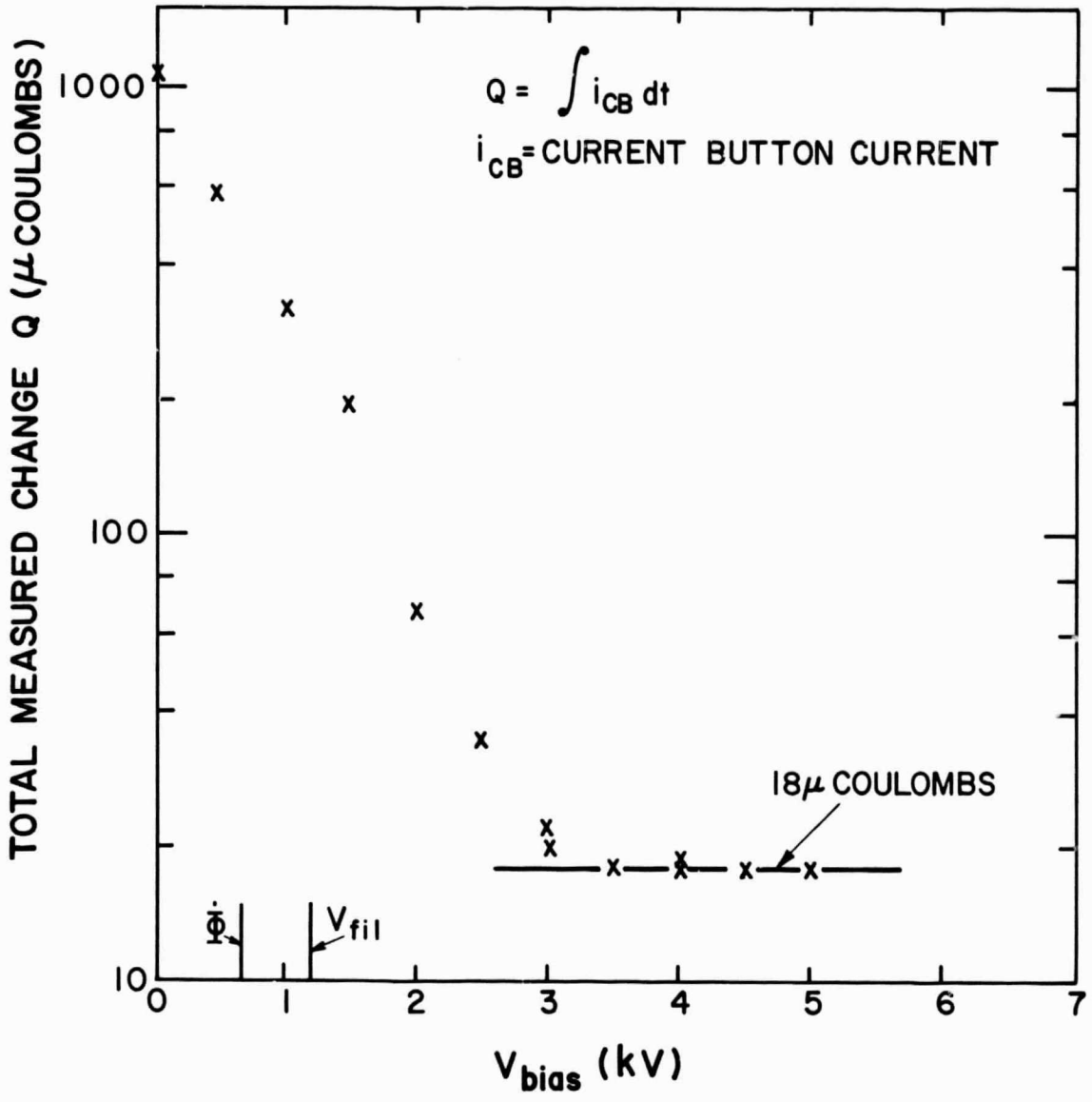

Fig. 4 Typical current button bias curve. This curve demonstrates that as the current button is biased negative, excess electron losses from the injection beam are prevented from reaching the current button. The plateau in the measured charge reached as the larger negative biases represents the image of the true injected charge.

an electron cloud instability but rather are induced by our continuing attempt to inject the cutoff electron beam (Section 4). However, the occurrence of these waves has provided us with a very useful diagnostic method. We have found empirically that for the $\ell = 1$ fundamental diocotron oscillation mode[4] the small amplitude oscillation frequency f_1 is directly proportional to the total injected charge. Thus we have found that

$$Q \approx (8\pi^3 R_o^2 \epsilon_o B_o) f_1, \tag{3}$$

where B_o is the magnitude of the magnetic field at the major radius, R_o, of the torus. Equation (3) can be interpreted as the statement that the $\ell = 1$ phase velocity is equal to the average zeroth order E/B speed at the wall of the apparatus. Levy[13] has provided a theoretical justification of this result for an infinite cylindrical apparatus with an arbitrary density distribution. Figure 3b, shows a typical set of small amplitude $\ell = 1$ mode traces obtained during an experiment. On Fig. 3b, a phase shift of nearly 180^o can be seen between the oscilloscope traces for current button A and current button B (see Fig. 2). We have reason to believe that the small discrepancy from a perfect 180^o phase lag results from a toroidal effect. An important outstanding problem for us is the generalization of this very powerful, small amplitude diagnostic technique to use with arbitrarily large amplitude waves and to use for arbitrary experimental cross section.

3. INDUCTIVE CHARGING

A. Conceptual Description

The basis of the inductive charging scheme[1] derives from the fact that in the guiding center approximation both the electrons and the flow of magnetic flux lines in an inductor move in the direction of Poynting's vector with the common velocity $(\underset{\sim}{E} \times \underset{\sim}{B})/B^2$. In a two dimensional cylinder, this common $\underset{\sim}{E} \times \underset{\sim}{B}/B^2$ velocity assures that, following the $\underset{\sim}{E} \times \underset{\sim}{B}$ motion, the quantity n/B = constant--while in an azimuthally symmetric, toroidal magnetic field the quantity nR/B is conserved. In these expressions n is the electron density, R the radius from the axis of the torus and B the magnetic field magnitude. Conservation of these quantities implies conservation of the total number of electrons in a flux tube. Thus, the common $\underset{\sim}{E} \times \underset{\sim}{B}/B^2$ motion of electrons and flux tubes assures that if a flux tube is initially "loaded" with electrons as it enters the inductor, then unless the adiabaticity of the electrons is violated, a rising magnetic field will carry a current of un-neutralized electrons into the device. Accumulation of this crossed field beam current within the conducting walls of the compression chamber produces a space charge cloud and a potential well.

Prediction of just what space charge distribution and what potential well will be produced by this process requires detailed knowledge of the $\underset{\sim}{E} \times \underset{\sim}{B}$ motion of each flux tube subsequent to its entering the compression chamber. Typical electric fields within the compression chamber are shown schematically in Fig. 5. In Fig. 5, we have shown only the fields appropriate

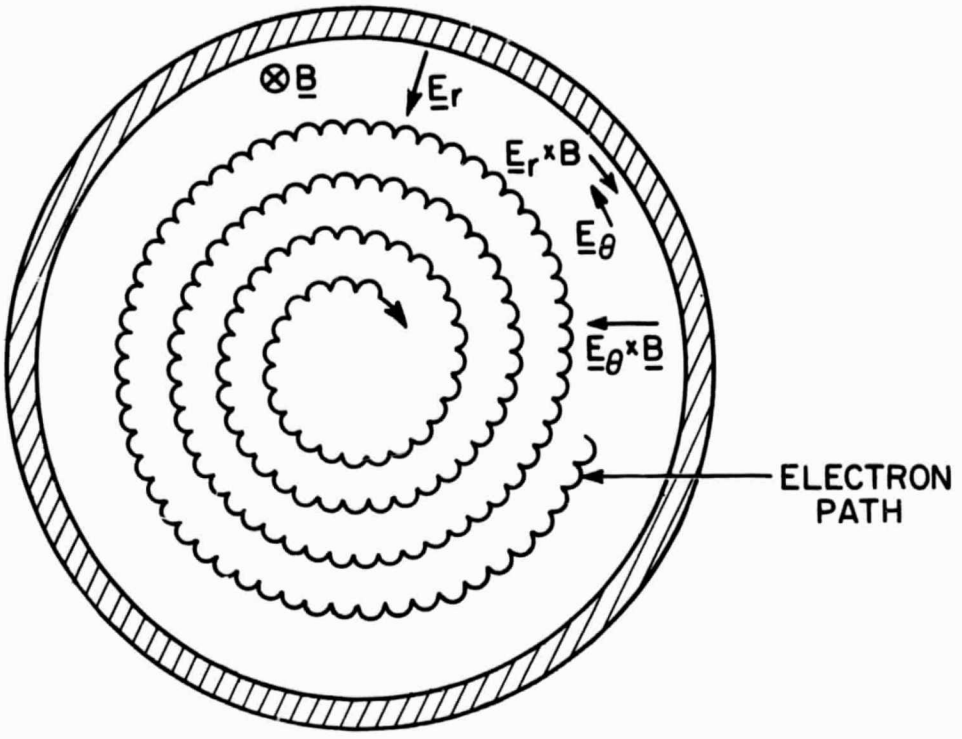

Fig. 5 This figure illustrates the principle of inductive charging. When the magnetic field is steady the only electric field is the radial field E_r due to space charge, and the only drift is the azimuthal drift E_r/B_z. When B is time varying an induced azimuthal electric field appears, $E_\theta \simeq rB/2$, at radius r. This electric field yields a radial drift speed $E_\theta/B_z = rB/2B$. This drift is inwards when B is increasing and vice versa. Since this radial speed will normally be small compared to E_r/B, the electron paths will resemble tightly wound spirals.

for a circularly symmetric cylinder (i. e. without a slot) since they provide the simplest demonstration of the inductive charging process. There are two significant electric fields: (1) E_θ due to the induction of the B field, and (2) E_r due to the electron space charge. E_θ produces a radially inward $\underset{\sim}{E}_\theta \times \underset{\sim}{B}/B^2$ drift motion while $\underset{\sim}{E}_r \times \underset{\sim}{B}/B^2$ produces a rotation. Combination of these motions results in the inwardly spiralling trajectory or path shown in Fig. 5 for a gyrating electron.

For more general configurations, it would at first appear that determination of the flux tube trajectory would be a difficult task. However, the electric fields in the compression chamber arising from induction of the magnetic field are only of the order of 10 volts/cm and so are very small in magnitude when compared with our final space charge electric fields--typically in excess of 10^4 volts/cm. Therefore, it is apparent that even very early in the injection cycle the "radial" space charge fields dominate the common $\underset{\sim}{E} \times \underset{\sim}{B}/B^2$ velocity of the electrons and the flux tubes. Thus again an electron trajectory rapidly rotates inside the device, slowly compressing "radially" due to the induction fields. This rapid rotation permits us to speak of a second adiabatic invariant. This invariant[12] is the total flux Φ inside the nearly cyclic path that an electron guiding center follows (adiabatically this path is considered closed). These adiabatically "closed" surfaces are the equipotentials of the space charge cloud. The electron cloud thus "winds up on itself" as the magnetic field is increased, placing newly injected flux tubes on the outside of the cloud and the nested equipotentials of the space charge cloud are surfaces enclosing constant total flux Φ.

The above discussion may be used to theoretically estimate the charge density distribution from the injection history. If during injection the injection current $I_{inj}(t)$ and the induction voltage $\dot{\Phi}(t)$ are known as a function of the total instantaneous flux $\Phi(t)$ in the device, then we can explicitly construct the function $g(\Phi(t)) = I_{inj}(t)/e\dot{\Phi}(t)$. Since each electron adiabatically conserves the total flux Φ inside its guiding center path it is shown in Appendix A that

$$g(\Phi) = \frac{I_{inj}(\Phi)}{e\dot{\Phi}(\Phi)} = \begin{cases} 2\pi(rn/B) & ; \text{ axisymmetric torus} \\ \ell\,(n/B) & ; \text{ two dimensional cylinder of length } \ell \end{cases} \quad (4)$$

Using one of these relations, the density distribution must be determined self consistently from Poisson's equation so that the flux surfaces Φ = constant used with Eq. (4) are also electrostatic equipotentials. Simple injection histories, such as $I_{inj}/\dot{\Phi}$ = const can be easily solved theoretically. Two dimensional circular cylinders with cylindrically symmetric flux surfaces ($\Phi = B\pi r^2$) yield cylindrically symmetric equipotentials and so also easily yield theoretical results even for non constant injection histories. Because of the small radius ratio ($a/R_o \approx .2$) of our present torus, the approximation of a two dimensional cylinder has been widely used in analyzing our data.

Implicit in the above discussion has been the assumption that during compresssion the electron cloud remains "centered" about an equilibrium with no large amplitude fluctuation. We should therefore amplify our remarks by noting that there is evidence that the inductive charging process tends to "center" the electron cloud. This has been demonstrated by Lowder[14] for an azimuthally symmetric injection scheme such as shown in

Fig. 5. Since diocotron waves[4] describe the time dependent $\underset{\sim}{E} \times \underset{\sim}{B}$ displacement of an electron cloud about an equilibrium, Lowder considered the effect of magnetic field induction on the amplitude of a diocotron wave. He has shown that the wave amplitudes are decreased by increasing the magnetic field. Our present experimental evidence reported in Section 5 supports this conclusion.

B. Experimental Observations of Injection Current

Figure 3a shows a typical image current oscilloscope trace as measured using a biased current button. This trace was taken with constant V_{fil}. The magnetic field starts at zero for t = o and rises as $B = B_{max} \sin(t/\tau)$ where $\tau \approx 25\mu$ sec. Thus, $\dot{\Phi} = \dot{\Phi}_{max} \cos(t/\tau)$. In this section, we wish to call attention to three characteristic features of this image current trace. In Section 3c we will provide a detailed explanation of these experimental observations.

The first characteristic feature is the initial rise in image current occuring shortly ($t = t_H$) after the magnetic field has started to rise. This delayed rise in injection current is explained in Section 3c as the occurrence of the Hull[15] "cutoff", a familiar phenomenon in crossed field devices.

The second feature we observe is the occurrence of a "plateau" or flat region in the injection trace. Comparison of this injection current plateau amplitude (I_p) with the total crossed field beam current, I_b, emitted from the filament indicates that I_p is typically only 5% to 10% of I_b. This loss of beam current can be explained as the operation of a natural electron energy limitation (Section 3c).

The third characteristic feature is the decrease in injection current which begins at a time t_c as labeled in Fig. 3a. From this time, the injection

current progressively decreases to zero. This gradual loss of the injection current is believed to result from progressive electron heating via the occurrence of an anomalous crossed field beam noise.

C. Discussion of Experimental Observations

1. Hull Cutoff

The first limitation that is observed during the injection process is Hull[15] cutoff. Hull provided a criterion for this effect which has been observed in crossed-field devices for many years. The criterion applies to the process of electron emission from a cathode under the influence of crossed electric and magnetic fields; in our case it roughly determines when a crossed-field beam is formed. Stated simply, the Hull cutoff criterion requires that the magnetic field must be large enough so that an electron emitted from the cathode cannot reach the anode because of the bending effect which the magnetic field has on the electron motion. In a planar configuration the Hull cutoff criterion requires that at the filament, the magnetic field B_{fil}, must satisfy

$$B_{fil} > B_H \equiv \frac{1}{h}\sqrt{\frac{2V_{fil}}{e/m}} \tag{5}$$

for a crossed field beam to form. (In a system with cylindrical symmetry and with the spacing h between concentric anode and cathode a considerably larger field (≈ 2) than predicted by Eq. (5) is required to form a beam).[15]

Since early in the induction cycle $B_o \approx \dot{\Phi}\, t/\pi a^2$, Eq. (5) implies that before a time $t \approx t_H$, where

$$t_H = \frac{\pi a^2}{\dot{\Phi}\, h}\sqrt{\frac{2\,V_{fil}}{e/m}}\left(\frac{R_o}{R_{fil}}\right) , \tag{6}$$

essentially all electrons emitted from the filament are conducted away by striking the anode and so injection cannot take place. The toroidal factor (R_o/R_{fil}) in Eq. (6) relates the average magnetic field B_o at radius R_o to the filament magnetic field at radius R_{fil}. For our more complex electrode configuration we should not expect the criterion of Eq. (6) to be precise. However, we have labeled the characteristic time t_H in Fig. 3a using the planar assumption of Eq. (6). The rather close agreement between t_H and the time of onset of injection suggests the correctness of this interpretation. Despite the complex geometry, we have interpreted the close agreement shown in Fig. 3a to indicate that the space charge limited beam which was emitted from the filament in this experiment formed a virtual negative electrode, thus generating a pseudo planar electric field configuration.

2. Macroscopic Energy Limit

We can explain the observed occurrence of an injection current plateau ($I_{inj}(t) = \text{const.} = I_p$ on Fig. 3a) as well as the observed loss of the bulk of the crossed field beam current ($I_b \gg I_{inj}$) by means of a very general macroscopic limit governing the maximum possible instantaneous total injected charge. Consider the fact that upon emission from the filament, each electron drifts near the conducting wall of the chamber with the local guiding center drift speed, E/B. In addition, each electron has a gyration velocity $v_\perp$ which is related to its magnetic moment[8] μ by the relation $1/2\ m\ v_\perp^2 = \mu B$. The magnitude of μ is of course determined by earlier non-adiabatic processes--such as emission from the filament. These two motions, perpendicular to the magnetic field, combine to produce the total speed $E/B + v_\perp$

once each gyration. This speed, of course, implies that the electron attains a kinetic energy of magnitude $(m/2)\,(E/B + v_\perp)^2$ once each gyration. If the electron is to not strike the wall, the initial potential energy of the electron, eV_{fil}, must exceed the kinetic energy requirements. Thus, if $(E/B + v_\perp)_{max}$ is the maximum magnitude of this quantity around the conducting wall of the device, then if an electron is to be injected, the inequality

$$e\ V_{fil} \geq \frac{m}{2} \left(\frac{E}{B} + v_\perp \right)^2_{max} \tag{7}$$

must be satisfied. In Eq. (7) we have neglected an additional term $\frac{m}{2} v_{\parallel}^2$ -- i.e. the energy of motion parallel to the magnetic field since we believe that this energy is negligibly small for our present injection scheme.

Since in our device the drift speed E/B results from the electron space charge Q, Eq. (7) places an instantaneous upper limit on the total accumulated charge. Consider first the case where $v_\perp$ is negligible. Writing

$$\left(\frac{E}{B}\right)_{max} = \kappa \left(\frac{E}{B}\right)_{Average} = \kappa \frac{(Q/2\pi R_o)}{(2\pi\epsilon_o a)\, B_o} \tag{8}$$

where κ is simply a factor relating the maximum local E/B speed to the average E/B speed, then Eq. (7) requires that the instantaneous total injected charge Q is limited to

$$Q \leq \left(\frac{2B_o}{\kappa B_H}\right) \left(\frac{a}{h}\right) Q_o \simeq B_o \sqrt{V_{fil}} \tag{9}$$

The abbreviation B_H is given in Eq. (5). From Eq. (9), we see that for a cold electron beam, by making $(2\ B_o/\kappa\ E_H)$ large we can greatly exceed the simple electrostatic limit of Eq. (1) and so justify our use of the tapered gap.

Equation (9) may be used to explain our experimental observation of a plateau in the injected current as well as the observed loss of most of the

beam current. For the experimental condition of a constant V_{fil}, and thus a constant Q_o, differentiation of Eq. (9) yields the ideal injection current, I_o,

$$I_o = \frac{2}{\kappa}\left(\frac{a}{h}\right)\frac{Q_o}{B_H}\frac{dB_o}{dt} \propto \frac{1}{\kappa}\sqrt{V_{fil}}\ \dot{\Phi} \ . \qquad (10)$$

Calculation with Eq. (10) using $\kappa = 1$, produces a magnitude for I_o which is much smaller than the total beam current ($I_o \ll I_b$) actually measured in the experiment of Fig. 3a. Thus, the discrepancy between I_b and I_{inj} can be an indication of the occurrence of the energy limitation.

If we assume that the energy limit is setting the magnitude of the plateau in the injection current, I_p, then we should find that $I_p \approx I_o$ as estimated theoretically. First, we took data to verify the dependence of I_p on $\sqrt{V_{fil}}\ \dot{\Phi}$ as is predicted by Eq. (10). This experimental data is plotted in Fig. 6. The data is well grouped by the correlation and the expected proportionality of I_p to $\sqrt{V_{fil}}\ \dot{\Phi}$ can be clearly seen. From the data in Fig. 6 we also calculated an empirical estimate of the factor κ -- $\kappa \approx 2.0$. It is possible to theoretically estimate the local electric field "stress concentration" factor for our experimental cross section as shown in Fig. 2. The peak electric field occurs at the rounded transition between the tapered electrostatic shield and the compression chamber. Combining the estimated electric field concentration factor with a theoretically estimated small toroidal correction (resulting from the fact that $n \propto \frac{B}{R}$ and $B \propto \frac{1}{R}$) we obtained a theoretical estimate of $\kappa \approx 1.9$--in very good agreement with the experimental results. Thus we believe that before the time t_c in Fig. 3a, we have been able to inject essentially all of the current theoretically possible.

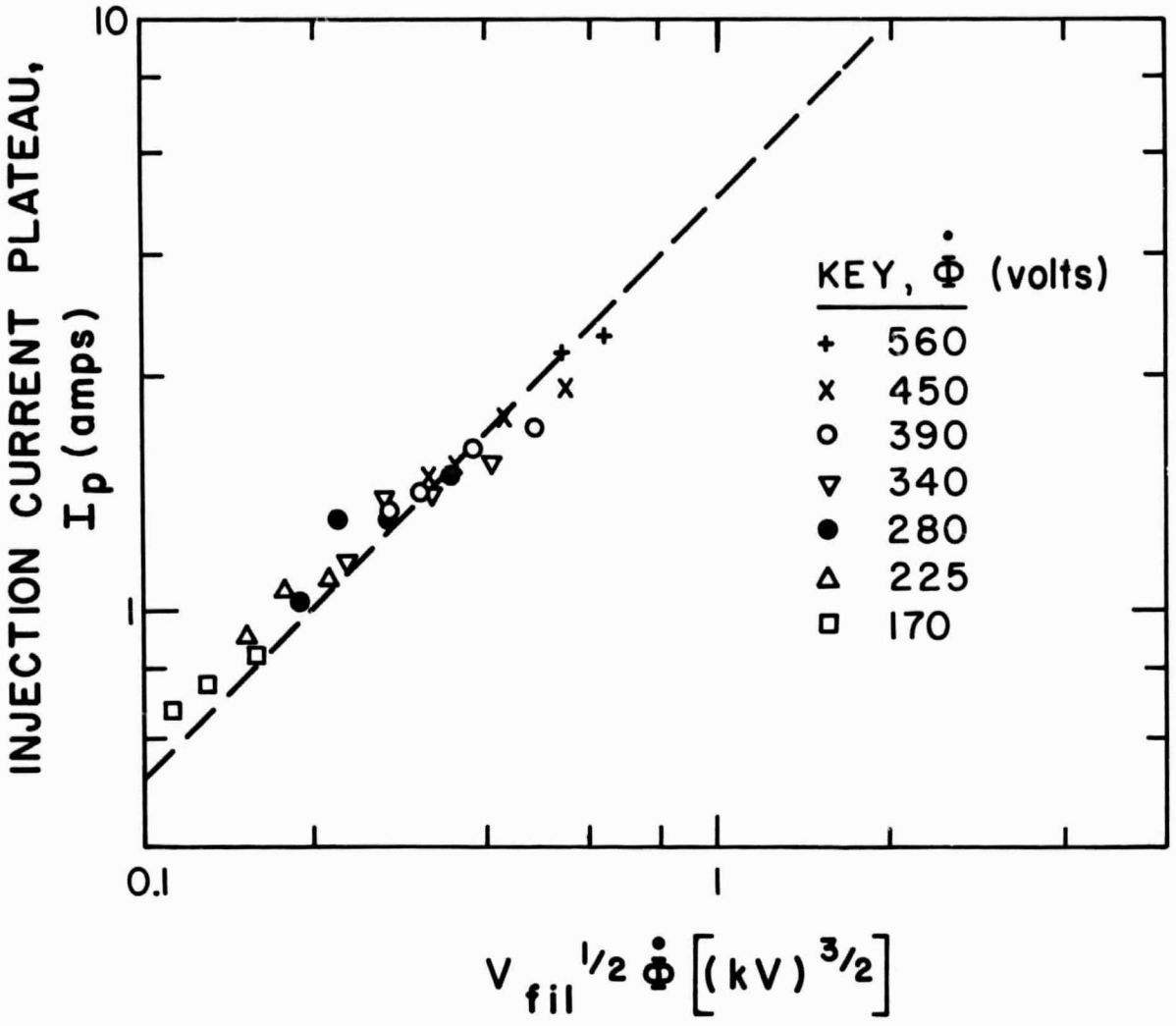

Fig. 6 Experimental correlation of the dependence of the magnitude of the plateau injection current, I_p (see Fig. 3a) as a function of $\sqrt{V_{fil}}\ \dot{\Phi}$. The electron energy conservation requirement that $eV_{fil} \geq \frac{m}{2}\left(\frac{E}{B}\right)^2$ suggests that the total charge in the system should be proportional to $B\sqrt{V_{fil}}$ and hence that $I_p \propto \dot{\Phi}\sqrt{V_{fil}}$ where V_{fil} is the filament bias voltage and $\dot{\Phi}$ is the induction voltage. The data is well grouped by this correlation.

Now consider the effect of a non-negligible $v_\perp$. We can define an instantaneous critical $v_\perp = v_c$ from the equality in Eq. (7). Doing this, find that the total charge Q is limited by the condition

$$Q = \frac{1}{\kappa}\left(\frac{2B_o}{B_H} - \frac{v_c}{(V_{fil}/hB_o)}\right)\left(\frac{a}{h}\right) Q_o \qquad (11)$$

Comparison of Eqs. (9) and (11) shows that for a given V_{fil}, the additional energy required to inject finite temperature electrons reduces the permitted total charge accumulation.

A further detail of the injection history may be inferred from Eq. (11) and an image current trace such as in Fig. 3a. If the "cold" electron injection expressed by Eq. (9) were followed precisely, then the image current trace should have actually overshot the plateau in Fig. 3a immediately after Hull cutoff at $t \approx t_H$. This overshoot in injection current would have been required to "make up" the total charge permitted by Eq. (9) but which was not actually injected before t_H. (Such an overshoot can actually be produced experimentally by introducing a delay in turning on the filament bias.) Thus, throughout the injection cycle in Fig. 3a, the total charge is actually slightly less than the maximum possible from Eq. (9) due to existence of a finite electron temperature. Using integrated current button traces, we can use Eq. (11) to estimate $v_c/(V_{fil}/hB_o)$. For typical injection histories electron temperatures of 100-200 electron volts have been estimated.

3. Anomalous Noise Limitation

The energy considerations given in the previous discussion suggest that very large charge accumulations should be possible with the inductive charging process--the only limitation being the magnitude of the maximum magnetic field. However, the image current trace shown in Fig. 3a clearly

demonstrates that injection begins failing after some critical time t_c during the injection cycle; ultimately injection ceases entirely. Thus, the experimental evidence shows that the current injection process is limited by an additonal (anomalous) mechanism.

The applied electric field used to extract electrons from the filament scales as V_{fil}/h. Therefore, a characteristic Larmor radius, r_E, is given by

$$r_E = \frac{V_{fil}}{h \frac{e}{m} B_{fil}^2} \quad \propto \quad \frac{V_{fil}}{h \dot{\Phi}^2 t^2} \tag{12}$$

Again, the approximation $B \propto \dot{\Phi}$ is valid for the times involved in the experiments. Thus, if we make the hypothesis that for a given experimental configuration a natural lower limit for the characteristic larmor radius, r_E, exists then the critical cutoff time should be correlated by

$$t_c \quad \propto \quad \left(\frac{V_{fil}}{\dot{\Phi}} \right)^{1/2} \tag{13}$$

The experimental data plotted in Fig. 7 was taken to test this hypothesis. The data was taken with constant V_{fil} during each experiment. We kept a constant filament spacing h and width w during the entire set of data. The data in Fig. 7 clearly shows a dependence of t_c on $\sqrt{V_{fil}}/\dot{\Phi}$. Thus, we believe the anomalous cutoff is due to a limitation on the characteristic larmor radius of the electron gun.

During the development of the Trochotron, a crossed-field switching device, Åström observed that for a given device, if the ratio $I_b B^2 / (V_{fil}/h)^{2.5}$ exceeded a certain critical value, then anomalous electron heating occurred and the crossed-field beam was lost to adjacent electrodes. Subsequent

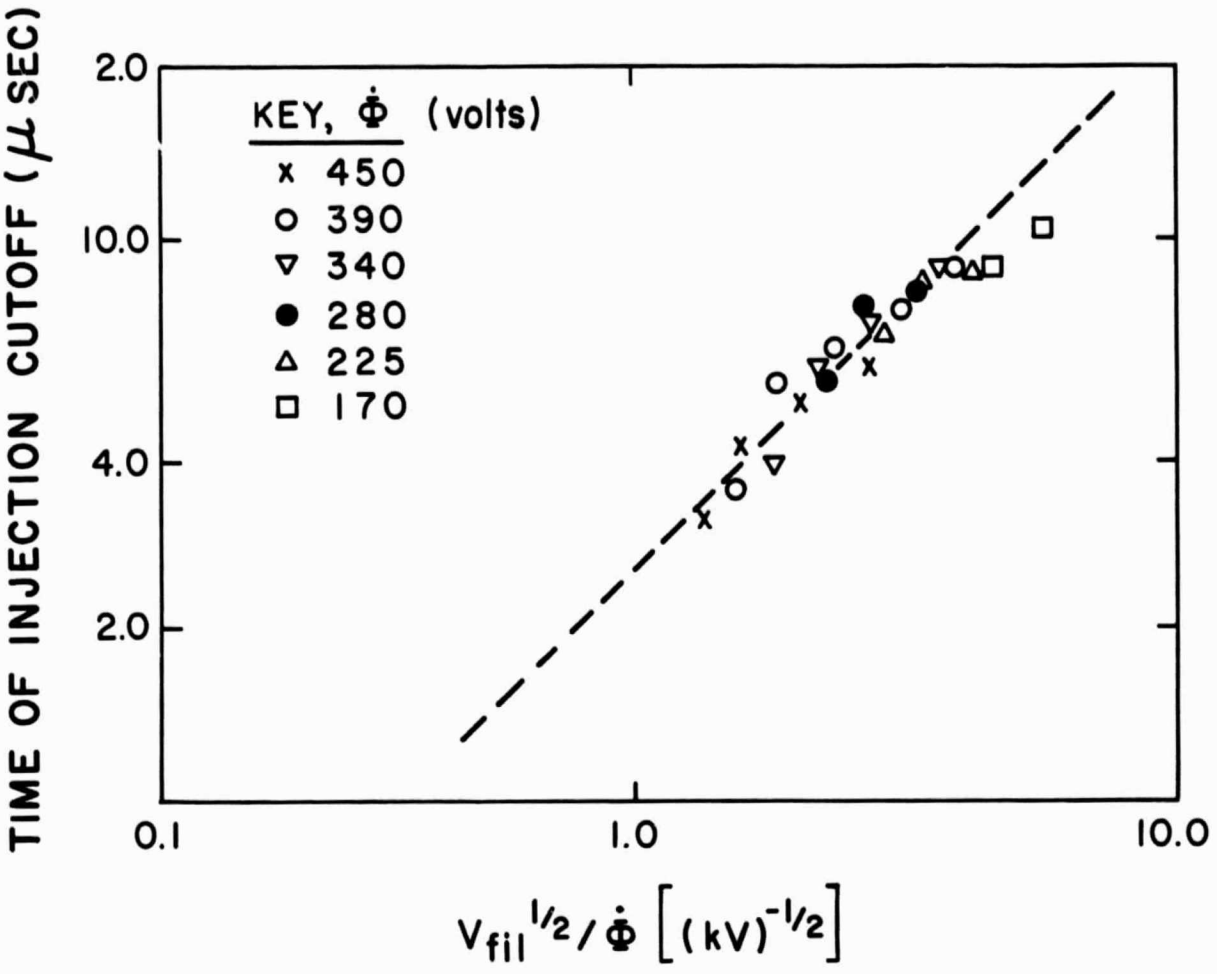

Fig. 7 Experimental data taken to determine the anomalous mechanism causing injection cutoff. The cutoff time t_c is correlated with $\sqrt{V_{fil}}/\dot{\Phi}$ for a wide range of parameters. In these experiments $B_{fil} \sim t$ and so this correlation is equivalent to the finding that injection fails when $B_{fil} > B_{critical} \sim \sqrt{V_{fil}}$; thus suggesting the anomalous cutoff results from the occurrence of crossed-field beam noise as observed in Refs. 10 and 16. Reference 17 finds noise occurs when the characteristic electron gyroradius at the filament $(mV_{fil})/(eB^2_{fil})$ becomes a fraction η of the filament width w. Our measurements yield close agreement, Eq. (15).

work on crossed-field beams for use in microwave devices, particularly by Miller,[10] further demonstrated these losses. An explanation of the phenomena has been advanced by Arnaud.[16] Arnaud suggests that if the characteristic Larmor radius r_E becomes a fraction η of the filament width w ($r_E = \eta w$), then noise oscillations and amplification are possible. This explanation applies to space charge limited emission (i.e. $I_b \propto V_{fil}^2/h^2B$) and involves a cross coupling of the crossed-field beam density fluctuations and fluctuations of the space charge potential minimum near the cathode. (We should note here that the assumption of a space charge limited beam also reduces Åström's criterion to the form of Eq. (12).) A recent paper by Arnaud[17] correlates the occurrence of anomalous noise with the condition that

$$\frac{V_{fil}}{\frac{e}{m} hwB^2_{fil}} \leq \eta \quad ; \eta \approx .3 \tag{14}$$

Using the experimental data in Fig. 7, we estimated the dimensionless ratio η for our experiments. We obtained a value of $\eta \approx 0.4$ which suggests that we are observing the occurrence of the same phenomenon as Arnaud et al. In our present experiment, the dependence of this correlation on h has been verified--particularly by the total charge measurements as given in Section 4. At this writing the dependence on w has not been verified.

In summary then, our experimental results show that we can inject until the magnetic field at the electron emitting cathode reaches a critical value of

$$B_{fil} = B_c \equiv \left(\frac{V_{fil}}{\eta \frac{e}{m} h w} \right)^{1/2}; \quad \text{where } \eta \approx 0.4 \tag{15}$$

After this critical magnetic field is reached, the injection current more or less gradually decreases to zero as seen in Fig. 3a. We interpret this decreasing current as resulting from the heating[9,10] of the electrons by the anomalous noise. Thus, from the discussion of the energy limit in Section 3c, we can readily see that if the anomalous noise heats essentially all of the beam electrons to such large perpendicular velocities that

$$\text{all } v_\perp > v_c \equiv \frac{V_{fil}}{h\, B_o} \left(\frac{2B_o}{B_H} - \left(\frac{\kappa\, h}{a} \right) \frac{Q}{Q_o} \right) \tag{16}$$

then injection will cease.

Possible means for improving on the limitation of Eq. (15) may be tested in the future. However, from consideration of the scaling laws as discussed in Section 6, and the possibility of programming the filament bias to satisfy Hull cutoff while still insuring that $B_{fil} < B_c$, we believe anomalous loss mechanism does not critically limit the injection process for the proposed applications.

PRECEDING PAGE BLANK NOT FILMED.

4. TOTAL CHARGE AND INDUCED ELECTROSTATIC POTENTIAL

A. General Results

In Section 3, we have described the energy limit which restricts the instantaneous total injected charge Q to less than a characteristic magnitude which is proportional to the instantaneous magnetic field. The maximum magnetic field at which we can inject is itself restricted by the anomalous noise limit.

Thus, these restrictions combine to determine the maximum total injected charge Q_{Total} in a given experiment. Consideration of Eqs. (9) and (15) shows that ideally

$$Q_{Total} \leq \frac{2}{\kappa} \left(\frac{R_{fil}}{R_o}\right) \sqrt{\frac{h}{2\eta w}} \left(\frac{a}{h}\right) Q_o \qquad (17)$$

$$\leq \frac{2.2}{\kappa} \frac{a}{\sqrt{hw}} \left(\frac{R_{fil}}{R_o}\right) (2\pi R_o)(2\pi\epsilon_o) V_{fil}$$

where we have accounted for the fact that for a toroidal magnetic field, $B \propto \frac{1}{R}$; and thus $B_o/B_{fil} = R_{fil}/R_o$. This ideal total charge restriction neglects the effects of finite electron temperature as well as of the charge injection accomplished after the noise limitation is reached i. e., after $t = t_c$ in Fig. 3a. Empirically, these effects appear to roughly compensate in our present experiments.

The semi-empirical limit Eq. (17) shows two characteristic features which we have specifically checked. First Q_{Total} should be proportional

to V_{fil} and second Q_{Total} should be inversely proportional to $\sqrt{h}$. The experimental data plotted in Fig. 8 was taken to check this dependence. In taking this data, our diocotron wave frequency technique for measuring total charge (Eq. (3)) has proven particularly useful. From our previous results we should expect to measure

$$f_1 \propto \frac{Q_{Total}}{\dot{\Phi}} \propto \frac{\bar{n}_e}{\dot{\Phi}} \propto \frac{1}{\sqrt{h}} \frac{V_{fil}}{\dot{\Phi}} \qquad (18)$$

if the fundamental ($\ell = 1$) diocotron wave frequency f_1 is measured at maximum magnetic field in each experiment. The linear dependence of $\bar{n}_e/\dot{\Phi}$ on $(V_{fil}/\dot{\Phi})$ is clear for both curves I and II. Between taking data for curve I and curve II, the filament spacing h was changed by a factor of 2. The change in slope between I and II is ≈ 1.4 thus confirming the expected dependence as $h^{-1/2}$.

The highest ratio of $(V_{fil}/\dot{\Phi})$ at which we have successfully injected is $V_{fil}/\dot{\Phi} \approx 3$. We have found that in order to achieve successful injection it has been necessary to emit sufficient total current from the filament that nearly a space charge limited beam is formed, i. e., $I_b \propto V^2_{fil}/h^2B$. For example, to achieve our best injection result of 52 μ coulombs at $V_{fil} \approx 2.4$ kv and h = 1.5 mm, it was necessary to emit ≈ 350 amperes peak current from our filament. Of this current, only about 20 amperes was actually injected. We obtained poorer injection results (by a factor of as much as 2) when insufficient current was emitted from the filament (i. e., filament was emission limited.) The precise reason for the poorer results obtained with an emission limited filament is not understood. Since the total current leaving the filament is measured, and it is greatly in excess of the actual injected current, it is clear that the reduction in total charge injected

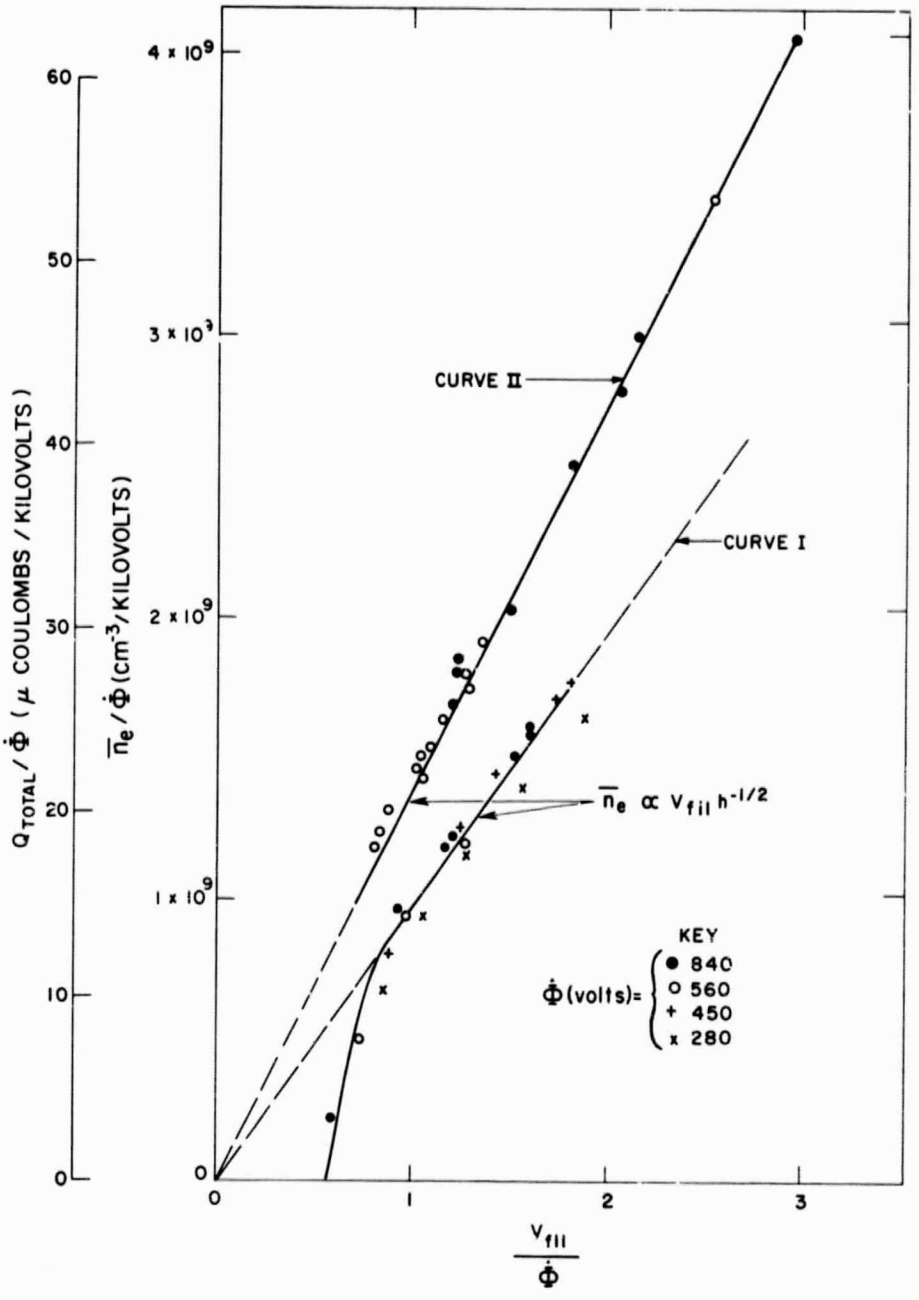

Fig. 8 Measurement of total injected charge as a function of $V_{fil}/\dot{\Phi}$ taken by the diocotron wave frequency technique (Eqs. (3) and (18)). Since the injection current is proportional to $\dot{\Phi}\sqrt{V_{fil}}$ and the cutoff time is proportional to $\sqrt{V_{fil}}/\dot{\Phi}$, one would expect the total charge to be proportional to V_{fil}, the filament bias voltage. For $V_{fil}/\dot{\Phi} \leq 3$ the total injected charge is shown to be proportional to V_{fil} and inversely to $h^{1/2}$. The maximum injected charge achieved is 52μ coulombs corresponding to an average electron density of $\approx 4 \times 10^9$ cm^{-3}. Curve I was taken with a filament spacing, h, of 3 mm. Curve II was taken with a spacing of 1.5 mm. The increased yield, for a given V_{fil}, but smaller h results from an increase with critical cutoff time, t_c, due to the stronger electric field in the region of the filament, ($\Omega \sim V_{fil}/h$).

does not result from electrons "circling" the compression chamber and then striking the filament. Rather it seems probable from the energy limit discussion of Section 3 C. 2 that the reduction in total charge injected results from the occurrence of excessively high electron temperatures.

B. Uncompressed Density and Voltage

Our best experimental result has been the injection of $\approx 52\mu$ coulombs for a V_{fil} of 2400 volts and a $\dot{\Phi}$ of 800 volts. At injection cutoff, this total charge corresponds to an average electron density of $\approx 4 \times 10^9$ cm^{-3} completely filling the device. At such cloud densities, direct measurement of the induced electrostatic potential by voltage probes has not been possible. However both from the assumption of a uniform charge density as well as from extrapolation of voltage measurements taken at lower electron densities, we have inferred that the uncompressed well depth was $V_{well} \approx 170$ kv for this experiment,

C. Compressed Density and Voltage

After injection cutoff the continuing rise in magnetic field compresses the density of electrons in the device (nR/B = const. as discussed in Section 3 a). Magnetic field compression ratios of 3 to 5 have been typical. By such cloud compression, electron densities in excess of 10^{10} cm^{-3} have been produced. Both theoretical and experimental evidence show that the injected electron cloud compresses about a "centered" equilibrium when we continue induction after injection cutoff. The location of the edge of this compressed cloud (dimension b in Fig. 9) may be estimated from knowledge of the total magnetic flux within the torus when injection stops. Thus the relative change in the electron cloud dimension from cutoff to complete compression is given by

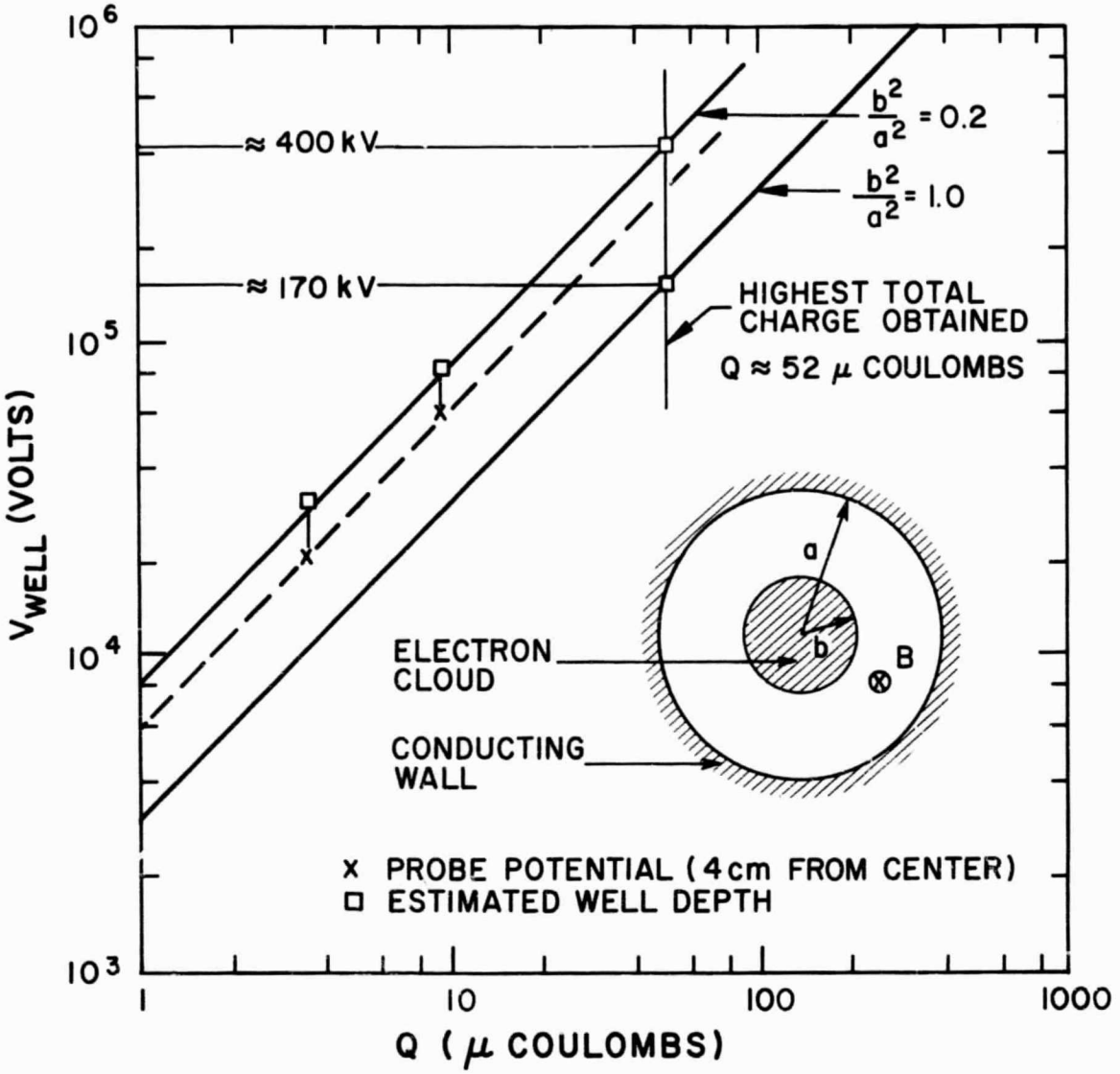

Fig. 9 Cross correlation of induced electrostatic well depth as a function of total injected charge Q and the degree of the electron cloud compression, b/a. The assumptions entering the theoretical lines are a uniform electron density out to a dimension b inside a circular cylinder of dimension a (as shown by the schematic insert). The experimental points are several direct probe measurements of well potential for small Q. The X's represent the potential measured at the predicted edge of the cloud (dimension b). The squares are the corresponding potential at the center of the electron cloud. These low voltage results show the validity of this cross correlation. The highest voltage, 400 kV, obtained is inferred from the point Q ≈ 52 μ coulombs and $(b/a)^2 \approx 0.23$. Probes could not be used for voltage in excess of 80 kV because of breakdown difficulties.

$$\left(\frac{b}{a}\right)^2 \approx \frac{(B_o)_{cutoff}}{(B_o)_{max}} . \qquad (19)$$

From our knowledge of the injection current such as Fig. 3a, we have estimated this ratio in the various experiments and so have estimated the peak induced voltage. Cross correlation of voltage probe measurements with total charge measurements as shown for low voltages (< 100 kv) in Fig. 9 show the validity of the technique. Thus for our "best" data of $\approx 52\mu$ coulombs we have obtained $V_{well} \approx 400$ kv. This result was obtained with a magnetic field compression ratio of ≈ 4.3 ($b/a \approx .48$).

5. CONTAINMENT

A. General Discussion

The prospects for long-time containment of electron clouds in toroidal magnetic fields depends upon satisfaction of three basic conditions:

a) The existence of an appropriate steady equilibrium,

b) The absence of instabilities on the time scales of interest,

and

c) Negligible classical diffusion losses.

In this section, we comment briefly on what is understood concerning each of these basic requirements. Subsequent sections will cover the experimental evidence as it relates to them.

1. Equilibria

For toroidal electron clouds, it has been shown theoretically[3] that steady, azimuthally symmetric, self-consistent equilibria should exist which accomplish a cancellation of the familiar toroidal gradient B and curvature drifts without the necessity of a magnetic rotational transform.

2. Instabilities

Three types of instabilities affecting electron clouds on the time scales of current experimental interest have been identified theoretically. These are the 1) diocotron instability,[4] 2) a "magnetron" instability[5] and 3) an ion-electron "two stream" instability.[12] The first of these instabilities has been avoided by proper selection of the electron cloud configuration.[2, 4] The magnetron instability has been avoided experimentally since

$q = \omega_p^2/\omega_c^2 \leq 1/100$ in our experiments; theoretical[5] and experimental evidence[1] indicate that a value of q greater that approximately 1/20 is required for the magnetron instability to be significant (ω_p = electron plasma frequency; ω_c = electron gyro frequency). The ion-electron "two stream" instability arises because of the progressive neutralization of the electron cloud by the ionization of the residual gas in the experimental apparatus ($p > 10^{-7}$ torr.) A theory[12] considers the electron cloud configuration shown in Fig. 10a. This theory accounts for the coupling between diocotron (electron) and ion wave motion; it predicts that an instability will occur when the fractional neutralization ($\alpha = Z\,\bar{n}_i/\bar{n}_e$) reaches a magnitude of the order of 10% to 20% (in the present experiments). Once instability is reached the growth rate is rapid--occurring on a time scale inversely proportional to the ion plasma frequency. From the theory, the magnitude of critical ionization fraction is found to depend upon 1) the effective ion mass (m_i/Z) (where Z is the charge state of the ion; Z = 1 in our present experiment) 2) the parameter q, and 3) the distance from the edge of the electron cloud to the highly conducting wall of the torus (i. e. the degree of compression, b/a, Eq. (19) and Fig. 10a). This model is idealized but yields satisfactory results for correlating our present experimental data. The theoretically[12] predicted critical values of fractional ionization are shown parametrically in Fig. 10b.

3. Classical Losses

Classical losses fall into two categories. The first arises from an energy principle. Once an ion is ionized it will "fall" into the electrostatic potential well. Individual ion motions are oscillatory. However time

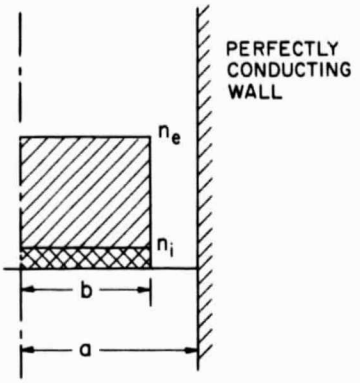

Fig. 10 (a)

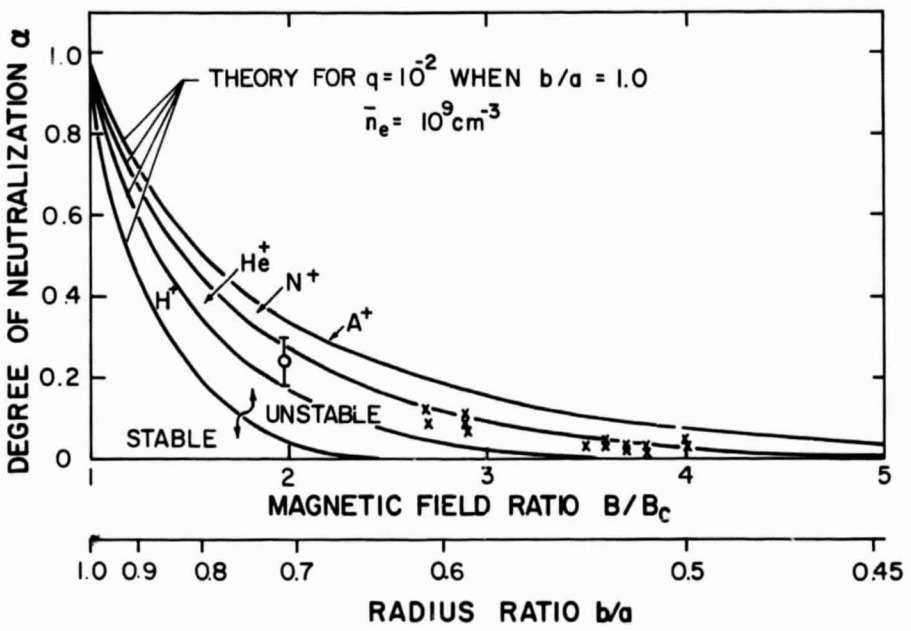

Fig. 10 (b)

Fig. 10 Theoretical predictions concerning an ion-electron "two stream" instability (Ref. 12). Figure 10a shows schematically the theoretical model which considers an electron cloud and an ion cloud both of dimension b continued within a conducting circular cylinder of dimension a. Guiding center motion is assumed for the electrons. The full ion dynamics are considered. Theory predicts an instability when the fractional neutralization ($\alpha = Z\, n_i/n_e$) reaches a critical magnitude dependent both on the dimensionless ratio b/a and the atomic species. For Z = 1 the theoretical predictions for α are shown in Fig. 10b. Experimental points are shown for experiments such as Figs. 12 and 13. As discussed in the text, the points compare with the theory for N^+.

averaging over all of the randomly produced ions results in a net time averaged gain in ion kinetic energy. This energy came from the electrostatic energy of the potential well. As the number of ions increases the potential well depth should decay on a time scale of several hundred microseconds to several milliseconds in our present experiments (depending upon the background pressure).

The second category of classical loss derives from the fact that short range collisions result in a "radial" diffusion of electrons, parallel to the "radial" space charge electric field. Because of the small electron gyro radius, this phenomenon is much too slow to have been influential in our present experiments--a time scale of 10 millisec or more would be required for significant diffusion to be observed.

B. Experimental Observations

Figure 11 shows a typical image current trace which was obtained with our lowest neutral gas pressure in the apparatus ($p \approx 4 \times 10^{-7}$ torr). In Fig. 11, we observe (1) injection, (2) a very quiescent period lasting for over 60μsec after injection cutoff and finally (3) rapid growth of an instability. The unstable wave has been observed to be the $\ell = 1$ diocotron wave by measuring the lack of any phase variation azimuthally around the major radius of the torus, as well as by phase measurements around the minor circumference. During the quiescent period, only very low amplitude steady waves are detectable.

Figure 12 shows a set of image current traces which were taken with a constant total injected charge to determine the dependence of the time of onset for the diocotron wave instability with (1) the background gas pressure and (2) with the degree of cloud compression as signified by the dimensional

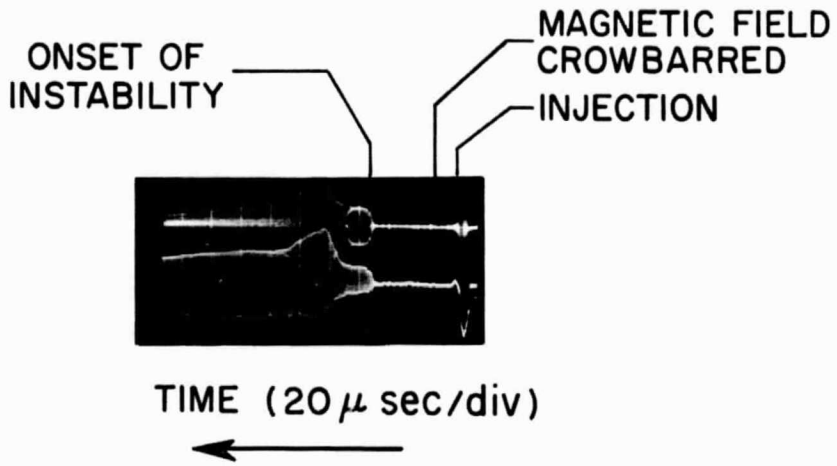

Fig. 11 Typical image current trace obtained with the lowest gas pressure in the apparatus ($p \approx 4 \times 10^{-7}$ torr). The quiescent period (no waves) observed in this trace extends for over 60μ sec. This quiescent period during which the electron cloud is "centered" to better than 1.5 mm is believed to be direct evidence for the existence of a stable toroidal equilibrium without the necessity for a magnetic field rotational transform. The difference in the detail of the two traces results from different frequency filtering of the detected signals.

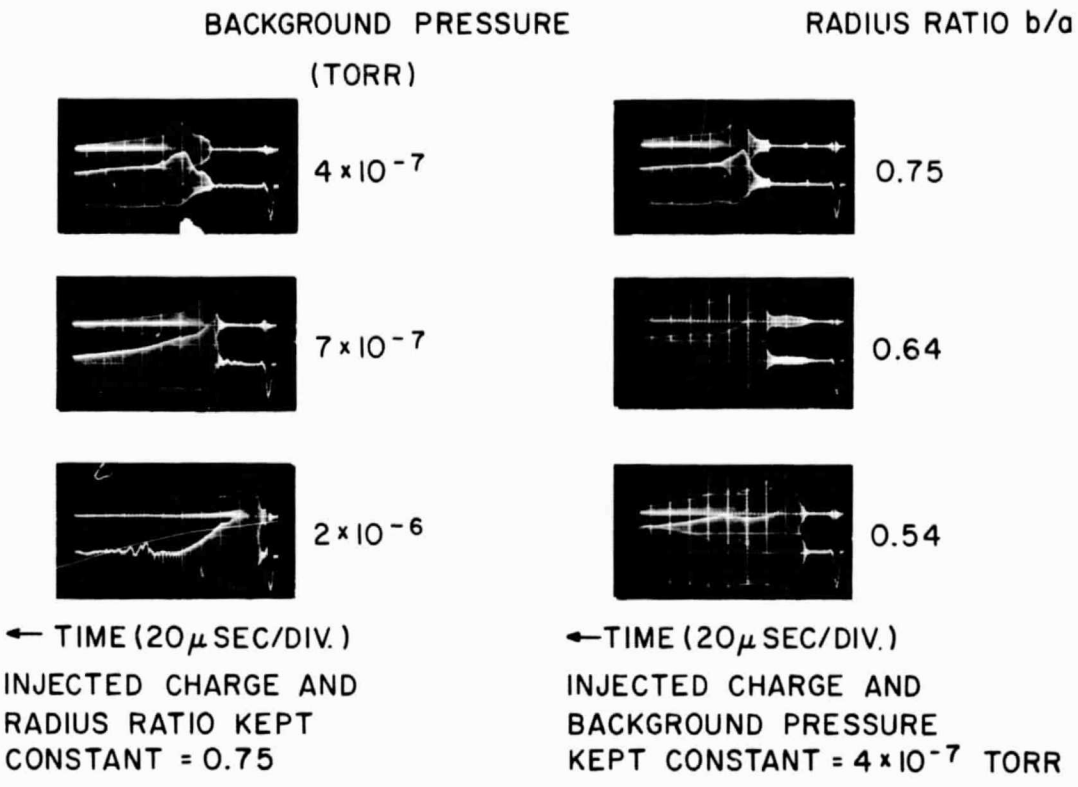

Fig. 12 Image current traces showing the variance of the time interval from injection to onset of the diocotron wave instability as a function of both background gas pressure and the dimensionless ratio b/a.

ratio b/a--the smaller b/a the larger the compression. In Fig. 12, we observe that as the neutral gas pressure is increased by adding nitrogen to the apparatus, the quiescent period shortens. We also observe that as the cloud compression increases, the quiescent period shortens.

The data shown in Fig. 13 was taken to determine the time of onset of the instability as a function of the residual background gas pressure in the device. Two different pressures are plotted for each onset time. The reason for this is the fact that with each experimental test, a pressure increase occurred due to the heating of the filament and/or from electron beam losses to the wall. At the higher pressures this pressure "burst" became insignificant and the data approach each other. For several reasons we believe the peak pressure to be the correct pressure for interpreting our results. Most important of these reasons is the fact that the linear slope of the higher pressure data points--common to both the peak and initial pressure measurements--extrapolates with the peak pressure data points at the lower pressures. Thus our discussion is based upon the peak pressure measurements.

Finally, we wish to return to the data of Fig. 3a, where $\ell = 1$ diocotron waves are observed to occur immediately after the injection cuts off. In this experiment, the filament was kept biased after injection cutoff and a crossed field beam was continuing to be emitted. During this time the wave amplitude is seen to grow. However, when the filament bias was removed at a time $t = t_b$, we observe that the $\ell = 1$ wave amplitude begins to decrease. This decrease can be explained by the stabilizing effect that a rising magnetic field has on a diocotron wave as discussed by Lowder[14] and mentioned in Section 3A. The wave growth occurring some time later is

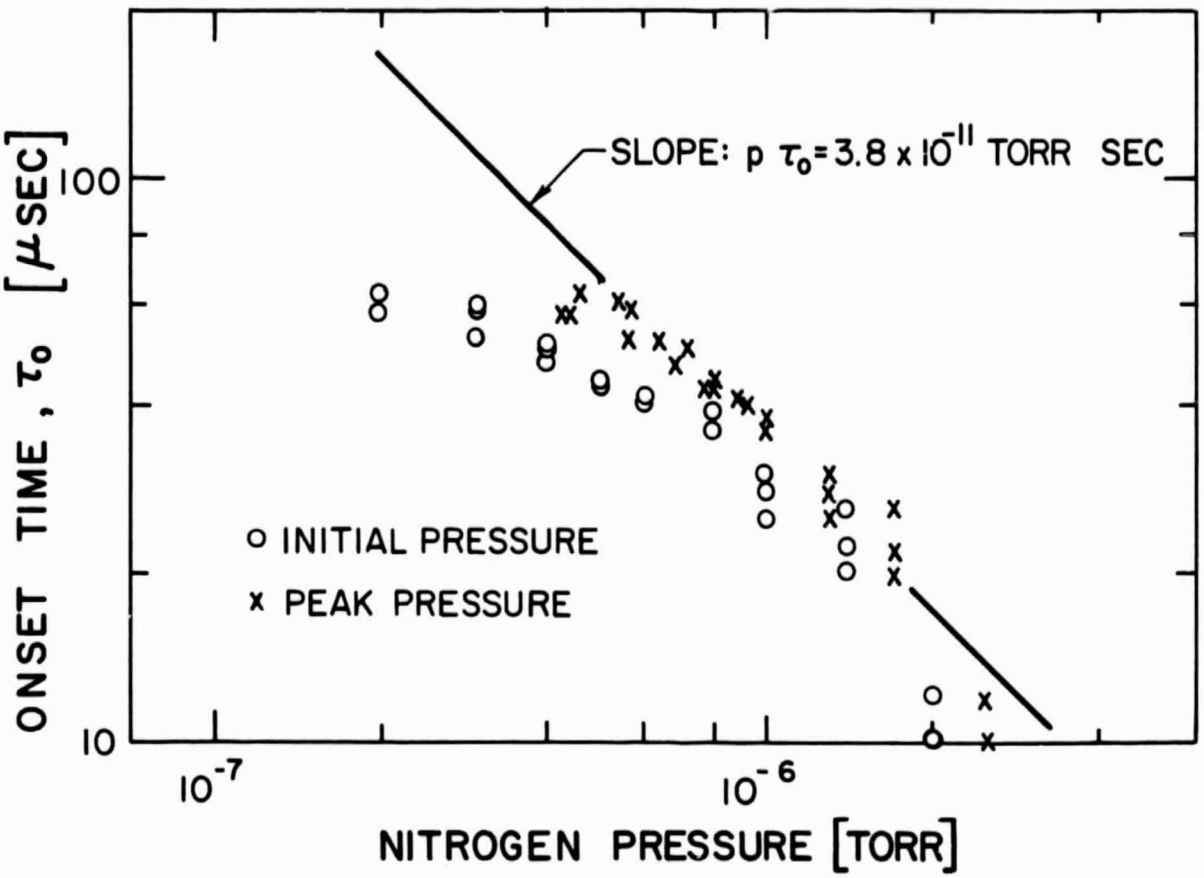

Fig. 13 Data taken to determine the dependence of the time of onset of the $\ell = 1$ diocotron wave instability as a function of the residual gas pressure in the device. Both the initial pressure existing in the apparatus before each experimental test and the peak apparatus pressure resulting from an outgassing burst during the experiment are shown. The linear correlation of the peak pressure data at both the higher and the lower pressures is believed to demonstrate the relevance of the peak pressure measurement in interpreting the occurrence of the diocotron instability. The inverse proportionality between onset time and pressure means that the instability occurs when a critical ion density is reached.

due to ion formation as with the instabilities of Figs. 11 and 12. With a suitably low vacuum, inductive stabilization has been observed to decrease beam induced diocotron waves to a very small amplitude, yielding a nearly quiescent state as in Fig. 11. The quiescent state in Fig. 11 was obtained by removing the filament bias at injection cutoff, thus avoiding generation of any beam induced waves.

C. Discussion of Experimental Observations

1. Equilibria

In Section 3d, we noted that the electron temperature ($k\,T_\perp = \frac{m}{2} v_\perp^2$) may be estimated from the injection history. Thus, for the data of Fig. 11, we have estimated that $k\,T_\perp / e > 100$ volts. The filament bias voltage, V_{fil}, was 900 volts in this experiment. Furthermore, because of the increase in magnetic field which occurs after injection, all electrons suffer an adiabatic heating of at least a factor of 2 in $k\,T_\perp$. Therefore, our estimate of 100 volts may be reasonably considered as a conservative lower bound. Furthermore, we believe that $k\,T_{||}$ is negligible for our present method of electron injection. Therefore, for $k\,T_\perp / e = 100$ volts, the axial guiding center drift velocity, v_z, due to the toroidal gradient B is given by[8]

$$v_z \approx \frac{1}{2} \frac{v_\perp^2}{R_o \omega_c} \approx \frac{k\,T_\perp}{R_o (eB_o)} \approx 1 \frac{mm}{(\mu\ sec)} \qquad (20)$$

For a quiescent period of 30 to 50 μ sec after the maximum magnetic field is reached, this drift would result in a displacement of $\approx$ 3 to 5 cm.

An upper limit on the actual displacement of the electron cloud during the quiescent period on the oscilloscope trace of Fig. 11 may be estimated. Any displacement of the cloud will produce a periodic rotation of this displacement within the apparatus. This rotation is the natural consequence

of the distortion of the surface charge distribution in the conducting walls of the container; this distortion arises from the cloud displacement and may be related to it. Figure 14 shows conceptually the effect of displacing the "center of charge" of an electron cloud in a two dimensional, circular cylinder. (A more precise description obtains from the consideration of diocotron waves; however, the results for $\ell = 1$ diocotron wave are quantitatively as well as qualitatively the same as for this conceptually simpler "center of charge" model.) The magnetic field is axial and we represent the "center of charge" of the electron cloud by a line charge of magnitude $-Q_1$ per unit length. Displacement of this line charge at small radial distance δ produces a radial electric field of magnitude $Q_1 \delta/2\pi\epsilon_o a^2$ at the "center of charge". This radial, image charge field produces an azimuthal $\underset{\sim}{E}_r \times \underset{\sim}{B}$ drift or cyclic rotation at the frequence f_1 of Eq. (3).

Any such rotation may be detected from waves in the image current trace. The displacement may be related to the detected image current amplitude, since the wave frequency is given by Eq. (3). Thus for the trace of Fig. 11, we find that

$$\delta < 0.15 \text{ cm} \qquad (21)$$

during the entire $> 60\ \mu$ sec quiescent period.

It follows from this estimate that no gradient B drift of the magnitude of Eq. (20) has occurred. The quiescent period observed in our image current traces is therefore believed to be direct evidence of our achievement of an azimuthally symmetric toroidal equilibria as has been theoretically predicted[3] to exist.

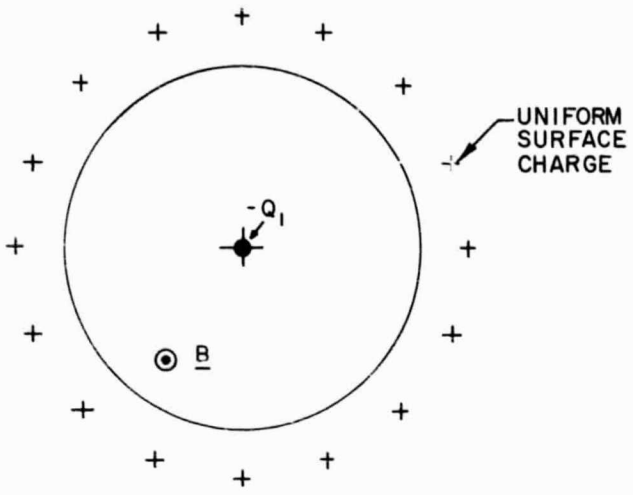

UNPERTURBED EQUILIBRIUM

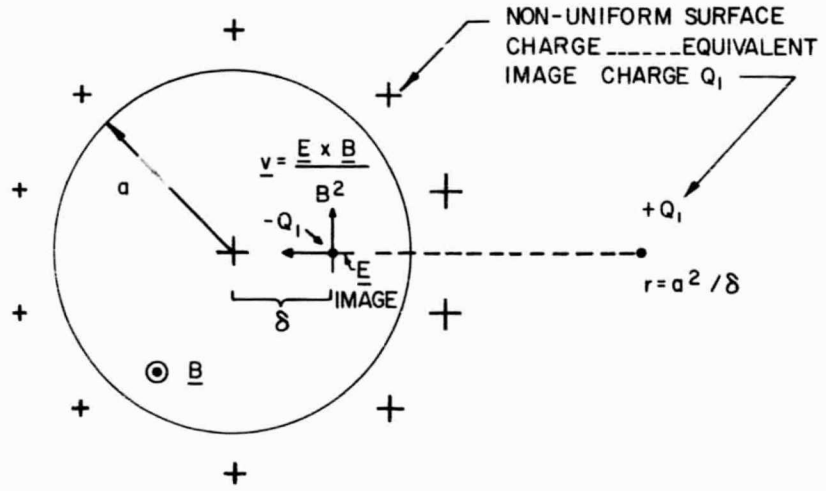

"OFF CENTER" CHARGE DISTRIBUTION

Fig. 14 Simple line charge model which demonstrates the correlation between the displacement of the center of charge of an electron cloud and the observance of waves on the current buttons. The displacement amplitude δ may be related to the amplitude of the observed current button signals.

2. Ion-electron "two stream" instability

The oscilloscope traces of Fig. 12 clearly show that the time interval from injection to the onset of the observed diocotron wave (ℓ =1) instability decreases as the pressure increases. The peak pressure data in Fig. 13 shows that the onset time is inversely related to the neutral gas density. On these time scales, classical diffusion losses are unimportant. Therefore, these facts suggest that the onset of the instability is related to the production of ions.

For a given residual gas in the apparatus, we may estimate the rate of ionization for our experiment conditions--that is $\dot{n}_i = n_n n_e (\sigma_i v_e)$. Hence the fractional neutralization, a, may be estimated as

$$a = \frac{n_i}{n_e} = n_n (\sigma_i v_e) t = 3 \times 10^{16} p (\sigma_i v_e) t \qquad (22)$$

where p is the vacuum measured in torr.

From this equation we observe that if an instability occurs in a given experiment at a specific critical fraction of neutralization (as say for the theory of Fig. 10), then the time for onset of the instability should vary inversely as the neutral gas pressure. This dependence is precisely the dependence of the data in Fig. 13.

Since the dominant species of residual gas was nitrogen we can also make a quantitative check of our experimental results with the theory of Ref. 12. Using $(\sigma_i v_e) \approx 2 \times 10^{-7}$ cm^3/sec for our electron energies in the range of 10^2 - 10^3 eV,[18] we find $a = 6 \times 10^9 (pt)$. From Fig. 13, $(pt) \approx 3.8 \times 10^{-11}$; therefore, we estimate a critical neutralization fraction $a_c \approx .23$ for this experiment. From calibration of our pressure measuring equipment we believe the accuracy of our pressure measurements to about $\pm$ 20%.

The above result can be compared with theory as shown by the circled point in Fig. 10b. As described in Section 4, the degree of compression, b/a, may be estimated from image current data. From the experiments of Fig. 13, $b/a \approx 0.7$; this estimate was used in plotting the circled point. From the close agreement of this point with the prediction for nitrogen, we see that all of the experimental data of Fig. 13 correlates well with theory.

Additional data points varying gas pressure and the degree of compression b/a, were also taken. These results are also plotted in Fig. 13 as "X" 's. These results also show a close agreement with theory--thus confirming the predicted dependence of the critical ionization fraction with the degree of compression.

From these results we believe that the instability which we have observed is due to an ion-electron "two stream" instability essentially as described in Ref. 12.

PRECEDING PAGE BLANK NOT FILMED.

6. IMPLICATIONS OF THE RESULTS

A. Electron Injection:

In the absence of the development of means for circumventing the injection cutoff discussed in Section 3 C. 3, the semi-empirical formula Eq. (17) represents the ideal limit on the total charge which can be injected. In this expression, there are two dimensions, a and h, over which we have a known control. Our best injection results were obtained with $h \approx 1.5$ mm, which is nearly a practical limit for our large filaments. With regard to changes in the dimension a, the specific objective must be considered. First, the induced potential well depth varies as Q and thus as the dimension a. Thus increasing a is clearly the direction to proceed to accomplish the very large potentials required of the space radiation shield[7] ($\sim$ 50 M volts) and may be the direction to proceed for the heavy ion accelerator.[2] The scale length a can be increased indefinitely provided sufficient magnetic energy is available. However, for the heavy ion source application, one finds that the product of electron number density and minor radius, na, is the significant parameter which should be increased for increased performance (ion production rate $\propto n^2a^2$). But since $n \propto Q/a^2 \propto 1/a$, nothing is to be gained in performance from varying a.

However, even retaining the present dimensions for h and a we have available two characteristic ratios which can be optimized by careful design. The first of these is the ratio κ of "peak" to average E/B speed at the wall of the apparatus. From consideration of other possible experimental

cross sections, we believe it is possible to reduce κ to the neighborhood of 1.0. Thus, a factor of 1.7 or so over our present results should be possible by a "simple" change of experimental cross section.

The second dimensionless ratio is R_{fil}/R_o which is now less than 1.0 ($R_{fil} < R_o$). By simply relocating the filament structure to the maximum rather than minimum apparatus radius we will make $R_{fil}/R_o > 1.0$. With the present apparatus this would result in an improvement of roughly 1.8 in total injected charge. How far this favorable radius ratio effect can be pushed is at present unknown. However, from the fact that the electron kinetic energies $\frac{m}{2} v_\perp^2 \propto R_{fil}/R_o$ and $\frac{m}{2} v_{||}^2 \propto (R_{fil}/R_o)^2$ are radius dependent we can infer that limitations do exist.

Overall, we believe that at least a factor of 3 improvement in total charge injected is possible without a change in scale size or in the applied cathode bias voltage.

A factor of over 10 increase in V_{fil} is possible within existing high voltage technology. However, our results have shown that as the voltage V_{fil} is increased, the filament emission current must also be increased. The required emission increases at least as fast as V_{fil}, the precise power law is at present unknown. This effect may result in a restriction on the maximum bias V_{fil} which can be profitably applied. However, we know that a factor of at least 2 and probably more can be accomplished by adjusting both V_{fil} and h ($\Omega \propto V_{fil}/\sqrt{h}$, $I_b \propto V_{fil}^2/h^2$).

Thus by combining the above effects we believe that electron densities well in excess of 10^{10} cm^{-3} are possible. If further study shows that it is possible to circumvent the filament emission limit effect, densities in excess

of 10^{11} cm^{-3} ($n > 3 \times 10 \times 4 \times 10^{9}$ cm^{-3}) should be attainable within existing high voltage technology.

B. Electron Containment

We would like to conclude this section with a few remarks concerning the influence of the ion-electron "two-stream" instability upon the proposed applied devices.[2, 6, 7] First, we do not believe that this instability will influence the proposed space radiation shield application[7] since in this application ions are not trapped and accumulated within the electrostatic potential produced by the magnetically confined electron cloud. However, in the proposed heavy ion accelerator and heavy ion source applications, ions are trapped and accumulated. Thus, this instability must be avoided by a suitable choice of parameters.

The available theory (Fig. 10b) predicts that if $b/a \approx 0.9$, a fractional neutralization of $\approx$ 10% may be expected to be contained. This 10% estimate was selected for purposes of discussion and appears to have a reasonable margin of safety. Our present electron densities of 4×10^{9} cm^{-3} would thus be stable if $Z n_i < 4 \times 10^{8}$ cm^{-3}. In particular for $Z = 1$, if we achieved a residual gas pressure of $\approx 10^{-8}$ torr in the present apparatus then we believe that we would "burn out" the available neutrals and thus contain ions until multiple ionizations have occurred (i.e., a time scale of many milliseconds). If the degree of ionization Z is increased in other experiments, one must correspondingly decrease the ion density n_i. This must be accomplished by further improvements in the vacuum conditions.

For both the proposed accelerator and source we may consider that $Z \approx 40$ and containment times of 1 to 10 sec are representative. Based on our previously discussed injection studies a density of $\approx 4 \times 10^{10}$ seems a conservative possiblity. Thus, containment of ion densities of

$\approx (4 \times 10^{10})\,(0.1)/40 \approx 10^{8}$ cm^{-3} should be feasible. However, these ions are only the "useful" ions. The ions resulting from residual background gas, are pollutants and thus may be otherwise restricted. For the heavy ion source application, it may be possible to segregate the desired ions from the pollutants using a selection method based upon the differing Z/A in the ionized state. Then pollutant densities of $\approx 10^{8}$ cm^{-3} or initial gas pressures of 3×10^{-9} torr should be acceptable.

For a successful [illegible] accelerator, however, a pollutant level of 10% or a density of 10^{7} cm^{-3} ($p \approx 3 \times 10^{-10}$ torr) is probably a necessity. Such initial gas pressures in the range of 10^{-10} torr are feasible with existing high vacuum technology.

For the long 1 to 10 sec containment times required in the accelerator and source applications, the continual outgassing of the walls during this long time also places a restriction on the vacuum conditions. For a surface to volume ratio of ≈ 0.1 cm^{-1}, a pollutant density of 10^{7} cm^{-3} would be accumulated in 3 sec with an outgassing rate of 10^{-12} torr liter/cm^{2} sec. Outgassing rates of $< 10^{-12}$ torr liter/cm^{2} sec have been achieved without bakeout.[19] Thus we believe that our present results do not require vacuum conditions in excess of present technology.

7. CONCLUSIONS

We have conducted experiments on the injection and containment of clouds of unneutralized electrons in a toroidal apparatus. We have studied in detail the inductive charging method of electron injection[1] and have shown that injection is governed by

a) a macroscopic energy limit relating the injection cathode bias potential, V_{fil}, to the kinetic energy requirements of the electron within the apparatus.

and b) by the occurrence of an anomalous crossed-field noise mechanism which we believe heats the electrons -- the excess heating causing a violation of the kinetic energy restriction.

These mechanisms have been shown to combine -- thus limiting the total injected charge to a proportionality with the filament bias potential.

Average electron densities of 4×10^9 cm^{-3} have been achieved which correspond to an electrostatic well depth of $\approx$ 170 kv. Extrapolation of these results, considering the scaling laws developed in the present studies, permits our prediction that more than an order of magnitude improvement in density and voltage should be attainable without a change in scale size. To accomplish our present results, however, it has always been necessary for us to operate our crossed field injection gun space charge limited ($I_b \propto V_{fil}^2 / h^2 B$). This effect will probably require further study if densities in excess of 10^{11} cm^{-3} are required. By continuing to raise the magnetic field after injection cutoff we have compressed our average densities to densities $> 10^{10}$ cm^{-3} and have thus achieved well depths of $\approx$ 400 kV.

Our containment experiments are believed to have exhibited the achievement of an equilibrium during injection. As predicted theoretically[3] this equilibrium is achieved without the necessity of a magnetic rotational transform. We have found that the loss of electron equilibrium, which we observed as an instability of the $\ell = 1$ diocotron wave[4, 12] depends upon the neutral gas density in the apparatus as well as on the degree of electron cloud compression after injection cutoff. These facts have been shown to correlate well with the predictions of an instability theory.[12] Extrapolation of these results, based upon our present understanding, allows us to predict that this instability can be avoided in the proposed applications using techniques consistent with current high vacuum technology -- i,e., achievement of residual gas pressures of $\approx 10^{-10}$ torr and surface outgassing fluxes of $<10^{-12}$ torr-liter/cm^2 sec.

8. ACKNOWLEDGEMENTS

With pleasure we acknowedge many useful discussions with H. E. Petschek, R. H. Levy, and R. S. Lowder.

9. REFERENCES

1. G. S. Janes, Phys. Rev. Letters 15, 135 (1965).

2. G. S. Janes, R. H. Levy, H. A. Bethe, and B. T. Feld, Phys. Rev. 145, 925 (1966).

3. J. D. Daugherty and R. H. Levy, Phys. Fluids 10, 155, (1967).

4. R. H. Levy, Phys. Fluids 8, 1288 (1965).

5. O. Buneman, R. H. Levy, and L. M. Linson, J. of Appl. Phys. 37, 3203 (1966).

6. J. D. Daugherty, L. Grodzins, G. S. Janes, and R. H. Levy, Phys. Rev. Letters 20, 369 (1968).

7. R. H. Levy and G. S. Janes, AIAA Journal 2, 1835 (1964).

8. H. Alfvén, Cosmical Electrodynamics, Clarendon Press, Oxford, (1950).

9. H. Alfvén, L. Lindberg, K. G. Malmfors, T. Wallmark and E. Åström Theory and Application of Trochotrons, Trans. Roy. Inst. Technol., Stockholm, (1948).

10. M. H. Miller and W. G. Dow, J. of Appl. Phys. 32, 274, (1961). E. Okress, ed.; Crossed-Field Microwave Devices, Academic Press, New York, N. Y. (1961).

11. L. Spitzer, Jr., Phys. Fluids 1, 253 (1958).

12. R. H. Levy, J. D. Daugherty, O. Buneman, Avco Everett Research Laboratory Research Report 302 (to be published).

13. R. H. Levy, Phys. Fluids, 11, 920, 1968.

14. R. S. Lowder, (to be published).

15. W. A. Hull, Phys. Rev. 18, 13 (1921).

16. J. Arnaud and A. O. Dochler, J. of Appl. Phys., 33, 234, (1962).

17. J. Arnaud, Annales de Radio electricite 19, 3, (1964).

18. S. C. Brown, Basic Data of Plasma Physics, Technology Press, John Wiley and Sons.

19. N. Milleron, IEEE Trans. Nucl. Sci. NS-14, 794, (1967).

PRECEDING PAGE BLANK NOT FILMED.

APPENDIX A

In this appendix we show that during inductive charging the adiabatic conservation of total magnetic flux Φ within nested electrostatic equipotentials ϕ provides the basis for determining the charge density distribution from the injection history. These results are an adiabatic and toroidal generalization of the exact correlation of the injection history with density distribution which has been previously demonstrated for inductive charging in a two-dimensional circularly symmetric cylinder.[2]

Adiabatic conservation of total flux Φ by the rapid guiding center motion, as described in Section 3 A, implies we may write

$$N = G(\Phi) \tag{1A}$$

for all time during injection. N is the total number of particles within a torus containing the total flux Φ. The surfaces of these nested tori are equipotentials of the space charge cloud. The number of particles ΔN in the volume ΔV between Φ and $\Phi + \Delta \Phi$ (and so between ϕ and $\phi + \Delta\phi$), is given by the integral

$$\Delta N = \int_{\Delta V} n \, dx^3 \tag{2A}$$

Hence, in an azimuthally symmetric torus

$$\Delta N = \int_{\Delta V} n\, 2\, \pi\, R\, dR\, dz = 2\pi \int_{\Delta V} \left(\frac{nR}{B}\right) B dR d z \qquad (3A)$$

Since the quantity nR/B is also conserved by the adiabatic guiding center motion, we may also write

$$g(\Phi) = 2\pi \frac{Rn}{B} \qquad (4A)$$

The integral in Eq. (3A) is over a volume ΔV such that Φ is constant; hence, we may write

$$\Delta N = \int_{\Delta V} g(\Phi)\, B\, drdz = 2\pi \frac{nR}{B} \Delta\Phi \qquad (5A)$$

or

$$G'(\Phi) = \frac{dN}{d\Phi} = 2\pi \frac{nR}{B} \qquad (6A)$$

Precisely the same line of reasoning yields

$$G'(\phi) = \frac{dN}{d\Phi} = \ell \frac{n}{B} \qquad (7A)$$

for a two dimensional cylinder of length ℓ.

Unclassified

Security Classification

DOCUMENT CONTROL DATA - R&D

(Security classification of title, body of abstract and indexing annotation must be entered when the overall report is classified.)

1 ORIGINATING ACTIVITY (Corporate author) Avco Everett Research Laboratory 2385 Revere Beach Parkway Everett, Massachusetts	2a REPORT SECURITY CLASSIFICATION Unclassified 2b GROUP

3 REPORT TITLE

Experiments on the Injection and Containment of Electron Clouds in a Toroidal Apparatus

4 DESCRIPTIVE NOTES (Type of report and inclusive dates)

Research Report 284

5 AUTHOR(S) (Last name, first name, initial)

Daugherty, J. D., Eninger, J. E., and Janes, G. S.

6 REPORT DATE	7a TOTAL NO. OF PAGES	7b NO. OF REFS
July 1968	59	19

8a CONTRACT OR GRANT NO. AF 49(638)-1553 b PROJECT NO. Project Task: 9752-01 c d	9a ORIGINATOR'S REPORT NUMBER(S) Research Report 284 9b OTHER REPORT NO(S) (Any other numbers that may be assigned this report) NYO-3863-7

10 AVAILABILITY/LIMITATION NOTICES

11 SUPPLEMENTARY NOTES	12 SPONSORING MILITARY ACTIVITY
	OFOSR - Office of Aerospace Research USAF - Washington 25, D. C.

13 ABSTRACT

Injection and containment of un-neutralized clouds of electrons has been accomplished with an azimuthally symmetric, toroidal, magnetic field. The confining magnetic field is produced within a conducting toroidal chamber. The induction of this magnetic field has been used to inject the electron cloud (inductive charging). Average electron densities of 4×10^9 cm^{-3} and peak electrostatic well depths of $\approx$ 400 kv have been achieved. Semi-empirical correlations are given which show the inductive charging scheme to be governed by an electron energy restriction and finally limited by the occurrence of anamolous crossed field beam noise. Stable equilibria, without the necessity of a rotational transform have been observed for times in excess of 60 μ sec. Correlation of the containment time observations with the predictions of a theoretical model for an ion-diocotron wave instability shows that the containment time is governed by the rate of ionization of the residual neutral gas ($p > 10^{-7}$ torr) in the apparatus. The correlation of theory and experiment appear to confirm the theoretical prediction that significant fractional charge neutralization (in the range of 10% to 20%) can be stably contained. Interpretation of these results suggests that significant improvement in both electron cloud density and containment time should be possible.

DD FORM 1 JAN 64 1473

Unclassified

Security Classification

Unclassified

Security Classification

14 KEY WORDS	LINK A		LINK B		LINK C	
	ROLE	WT	ROLE	WT	ROLE	WT
1. Electron Cloud Containment 2. High Voltage 3. Toroidal Containment 4. Crossed-Field Devices 5. Non-neutral Plasmas						

INSTRUCTIONS

1. ORIGINATING ACTIVITY: Enter the name and address of the contractor, subcontractor, grantee, Department of Defense activity or other organization *(corporate author)* issuing the report.

2a. REPORT SECURITY CLASSIFICATION: Enter the overall security classification of the report. Indicate whether "Restricted Data" is included. Marking is to be in accordance with appropriate security regulations.

2b. GROUP: Automatic downgrading is specified in DoD Directive 5200.10 and Armed Forces Industrial Manual. Enter the group number. Also, when applicable, show that optional markings have been used for Group 3 and Group 4 as authorized.

3. REPORT TITLE: Enter the complete report title in all capital letters. Titles in all cases should be unclassified. If a meaningful title cannot be selected without classification, show title classification in all capitals in parenthesis immediately following the title.

4. DESCRIPTIVE NOTES: If appropriate, enter the type of report, e.g., interim, progress, summary, annual, or final. Give the inclusive dates when a specific reporting period is covered.

5. AUTHOR(S): Enter the name(s) of author(s) as shown on or in the report. Enter last name, first name, middle initial. If military, show rank and branch of service. The name of the principal author is an absolute minimum requirement.

6. REPORT DATE: Enter the date of the report as day, month, year, or month, year. If more than one date appears on the report, use date of publication.

7a. TOTAL NUMBER OF PAGES: The total page count should follow normal pagination procedures, i.e., enter the number of pages containing information.

7b. NUMBER OF REFERENCES: Enter the total number of references cited in the report.

8a. CONTRACT OR GRANT NUMBER: If appropriate, enter the applicable number of the contract or grant under which the report was written.

8b, 8c, & 8d. PROJECT NUMBER: Enter the appropriate military department identification, such as project number, subproject number, system numbers, task number, etc.

9a. ORIGINATOR'S REPORT NUMBER(S): Enter the official report number by which the document will be identified and controlled by the originating activity. This number must be unique to this report.

9b. OTHER REPORT NUMBER(S): If the report has been assigned any other report numbers *(either by the originator or by the sponsor)*, also enter this number(s).

10. AVAILABILITY/LIMITATION NOTICES: Enter any limitations on further dissemination of the report, other than those imposed by security classification, using standard statements such as:

(1) "Qualified requesters may obtain copies of this report from DDC."

(2) "Foreign announcement and dissemination of this report by DDC is not authorized."

(3) "U. S. Government agencies may obtain copies of this report directly from DDC. Other qualified DDC users shall request through _____."

(4) "U. S. military agencies may obtain copies of this report directly from DDC. Other qualified users shall request through _____."

(5) "All distribution of this report is controlled. Qualified DDC users shall request through _____."

If the report has been furnished to the Office of Technical Services, Department of Commerce, for sale to the public, indicate this fact and enter the price, if known.

11. SUPPLEMENTARY NOTES: Use for additional explanatory notes.

12. SPONSORING MILITARY ACTIVITY: Enter the name of the departmental project office or laboratory sponsoring *(paying for)* the research and development. Include address.

13. ABSTRACT: Enter an abstract giving a brief and factual summary of the document indicative of the report, even though it may also appear elsewhere in the body of the technical report. If additional space is required, a continuation sheet shall be attached.

It is highly desirable that the abstract of classified reports be unclassified. Each paragraph of the abstract shall end with an indication of the military security classification of the information in the paragraph, represented as *(TS)*, *(S)*, *(C)* or *(U)*

There is no limitation on the length of the abstract. However, the suggested length is from 150 to 225 words.

14. KEY WORDS: Key words are technically meaningful terms or short phrases that characterize a report and may be used as index entries for cataloging the report. Key words must be selected so that no security classification is required. Identifiers, such as equipment model designation, trade name, military project code name, geographic location, may be used as key words but will be followed by an indication of technical context. The assignment of links, rules, and weights is optional

Unclassified

Security Classification